Variation in spatial population structure in the *Anopheles gambiae* species complex

Robert S. McCann[1], Jean-Paul Courneya[1], Martin J. Donnelly[2], Miriam K. Laufer[1], Themba Mzilahowa[3], Kathleen Stewart[4], Fiacre Agossa[5,6,7], Francis Wat'senga Tezzo[5], Alistair Miles[8]*, Shannon Takala-Harrison[1]*, Timothy D. O'Connor[9,10]*, Ag1000G Consortium[†]

*These authors contributed equally
[†]list of Ag1000G Consortium members: https://www.malariagen.net/project/ag1000g/

[1]Center for Vaccine Development and Global Health, University of Maryland School of Medicine, Baltimore, USA
[2]Deptarment of Vector Biology, Liverpool School of Tropical Medicine, Liverpool, UK
[3]Malaria Alert Centre, Kamuzu University of Health Sciences, Blantyre, Malawi
[4]Center for Geospatial Information Science, Department of Geographical Sciences, University of Maryland, College Park, USA
[5]Unit of Entomology, Department of Parasitology, Institut National de Recherche Biomédicale (INRB/Kinshasa), Kinshasa, Democratic Republic of the Congo
[6]U.S. President's Malaria Initiative (PMI) Evolve Project, Abt Associates, Rockville, USA
[7]Department of Environmental Health, School of Public Health, Faculty of Medicine, University of Kinshasa, Kinshasa, Democratic Republic of Congo.
[8]Genomic Surveillance Unit, Wellcome Sanger Institute, Cambridge, UK
[9]Institute for Genome Sciences, University of Maryland School of Medicine, Baltimore, USA
[10]Program for Health Equity and Population Health, University of Maryland School of Medicine, Baltimore, USA

Corresponding author: Robert S. McCann, rmccann@som.umaryland.edu, Center for Vaccine Development and Global Health, University of Maryland School of Medicine, Baltimore, USA.

Abstract

Anopheles gambiae, *Anopheles coluzzii*, and *Anopheles arabiensis* are three of the most widespread vectors of malaria parasites, with geographical ranges stretching across wide swaths of Africa. Understanding the population structure of these closely related species, including the extent to which populations are connected by gene flow, is essential for understanding how vector control implemented in one location might indirectly affect vector populations in other locations. Here, we assessed the population structure of each species based on a combined data set of publicly available and newly processed whole-genome sequences. The data set included single nucleotide polymorphisms from whole genomes of 2,410 individual mosquitoes sampled from 128 locations across 19 African countries. We found that *A. gambiae* sampled from several countries in West and Central Africa showed low genetic differentiation from each other according to principal components analysis (PCA) and ADMIXTURE modeling. Using Estimated Effective Migration Surfaces (EEMS), we showed that this low genetic differentiation indicates high effective migration rates for *A. gambiae* across this region. Outside of this region, we found eight groups of sampling locations from Central, East, and Southern Africa for which *A. gambiae* showed higher genetic differentiation, and lower effective migration rates, between each other and the West/Central Africa group. These results indicate that the barriers to and corridors for migration between populations of *A. gambiae* differ across the geographical range of this malaria vector species. Using the same methods, we found higher genetic differentiation and lower migration rates between populations of *A. coluzzii* in West and Central Africa than for *A. gambiae* in the same region. In contrast, we found lower genetic differentiation and higher migration rates

between populations of *A. arabiensis* in Tanzania, compared to *A. gambiae* in the same region. These differences between *A. gambiae*, *A. coluzzii*, and *A. arabiensis* indicate that migration barriers and corridors may vary, even between very closely related species. Overall, our results demonstrate that migration rates vary both within and between species of *Anopheles* mosquitoes, presumably based on species-specific responses to the ecological or environmental conditions that may impede or facilitate migration, and the geographical patterns of these conditions across the landscape. Together with previous findings, this study provides robust evidence that migration rates between populations of malaria vectors depend on the ecological context, which should be considered when planning surveillance of vector populations, monitoring for insecticide resistance, and evaluating interventions.

Background

Vector control interventions play a crucial role in preventing the transmission of malaria parasites and reducing the public health burden of malaria. These interventions have been associated with significant reductions in malaria parasite infection, uncomplicated and severe malaria burden, and all-cause child mortality [1-3]. In 2022, national malaria programs distributed 254 million long-lasting insecticidal nets (LLIN) and protected 62 million individuals through indoor residual spraying (IRS) according to the World Health Organization (WHO) [4]. Despite these efforts, malaria still causes approximately 600,000 deaths annually, and 95% of these deaths occur in the WHO Africa Region [4].

Vector control policies are typically set by national malaria programs in response to a variety of factors such as local epidemiology and ecology, as well as cost and funding [5-7]. These policies determine where interventions are implemented and the specific interventions used, including the types (e.g. LLIN, IRS, larviciding, etc.), formulations, and distribution methods [8, 9]. This situation forms a heterogeneous landscape of interventions, each of which may impact malaria vectors in different ways in terms of reductions in population size and selection pressures from insecticides that could lead to resistance. Furthermore, the coverage of vector control interventions varies between and within countries [10], exacerbating the potential for differential impacts on local vector populations. The consequences of this heterogeneous vector control depend on the extent to which populations in locations with different interventions or coverage are connected by gene flow, as the rate of gene flow would determine the potential for the impacts of interventions on local vector populations to spread beyond the targeted area and indirectly affect vector populations in other locations.

One approach for understanding gene flow between populations is to infer migration rates based on the genetic differentiation and geographic distance between the populations. Under a model of isolation-by-distance, genetic differentiation would be expected to increase with geographic distance [11] at a rate determined by the dispersal ability of individuals, which is expected to be constant across a homogeneous landscape [12]. However, dispersal ability across a heterogeneous landscape may vary considerably, resulting in populations that are genetically differentiated either more or less than would be expected under isolation-by-distance [12]. Recently developed methods to estimate these deviations from exact isolation-by-distance provide a geospatial visualization of potential corridors and barriers to migration [13, 14]. Using these methods to identify geographical regions with higher or lower migration rates between malaria vector populations could enable predictions of how vector control implemented in one location might indirectly affect vector populations in other locations. Specific examples could include the spread of adaptive alleles conferring insecticide resistance [15], source-sink dynamics [16, 17], or the distribution of future interventions based on genetic modification [18].

The dominant malaria vectors in Africa include *Anopheles gambiae*, *Anopheles coluzzii*, and *Anopheles arabiensis*, which are closely related species in the *A. gambiae* species complex [19]. All three species have large geographical ranges distributed across dozens of countries [20], and in each country the national malaria program independently determines vector control policies. Previous studies of population structure in these *Anopheles* species based on microsatellite loci have generally found relatively low genetic differentiation across thousands of kilometers, indicating less structured populations and high migration rates between locations [21]. However, regions with presumed barriers to migration between populations have also been identified, such as the Rift Valley Complex for *A. gambiae* [22], the Congo Basin tropical rainforest for *A. coluzzii* [23], and the Indian Ocean for *A. arabiensis* [24]. These findings indicate that migration rates between populations of malaria vectors are not uniform across their geographical ranges, but instead depend on the ecological context. Recently, the *Anopheles gambiae* 1000 Genomes (Ag1000G) Project produced whole-genome sequences (WGS) from samples of these species collected in several countries (https://www.malariagen.net/project/ag1000g/). Results of population structure analyses based on single nucleotide polymorphisms (SNPs) from the first [25] and second [26] phases of Ag1000G have provided further evidence that the migration rates in these species depend on the ecological context. Additionally, a comparison between *A. gambiae* and *A. coluzzii* suggests that species-specific ecological adaptations may result in differences in migration rates between species in the same region [26].

In the current study, we assessed population structure and estimated effective migration rates for *A. gambiae*, *A. coluzzii*, and *A. arabiensis* based on WGS data from the third phase of Ag1000G combined with additional, recently processed WGS data. We used principal components analysis (PCA) [26] and ADMIXTURE [27] to assess genetic differentiation between populations based on genome-wide SNPs for each of the three species. We then used the SNP data sets and the mosquito sampling locations to create migration surface maps using the Estimated Effective Migration Surfaces (EEMS) program [13] to visualize where the genetic differentiation between populations within each species was higher or lower than expected under uniform isolation-by-distance. In addition to these assessments of within-species variation in migration rates, we also compared EEMS outputs between species *A. gambiae* and *A. coluzzii* in West and Central Africa, and between *A. gambiae* and *A. arabiensis* in East Africa.

Results

Summary of whole-genome sequence data sets

We used the publicly available set of WGS data produced by the third phase of the Ag1000G Project, combined with WGS data from 170 additional *A. gambiae* from Democratic Republic of Congo (DRC) and Malawi, to assess population structure and infer migration rates for three species of malaria vectors in Africa. All sequencing was done on Illumina technology, and sequence reads for all specimens were aligned to the AgamP4 reference genome. Following quality assessment and quality filtration steps (https://malariagen.github.io/vector-data/ag3/ag3.0.html), the final Ag1000G phase 3 data set included 2,784 mosquitoes collected from natural populations in 19 countries. These specimens were assigned to a species (e.g., *A. gambiae*, *A. coluzzii*, or *A. arabiensis*) based on a PCA described in more detail at https://malariagen.github.io/vector-data/ag3/methods.html. We performed analyses separately for each of the three species, excluding specimens assigned to a cryptic taxon (n = 434) and those that appeared to be F1 hybrids (n = 5). We also excluded 75 *A. gambiae*, 21 *A. coluzzii*, and 2 *A. arabiensis* from sibling and parent-offspring kin-groups based on pairwise kinship coefficients using KING version 2.2.7 [27], because these highly-related individuals would

148 otherwise artificially deflate measures of within population genetic differentiation. Our final data
149 set for analysis included 1,565 *A. gambiae* from 107 unique geolocations in 17 countries (**Fig. 1**),

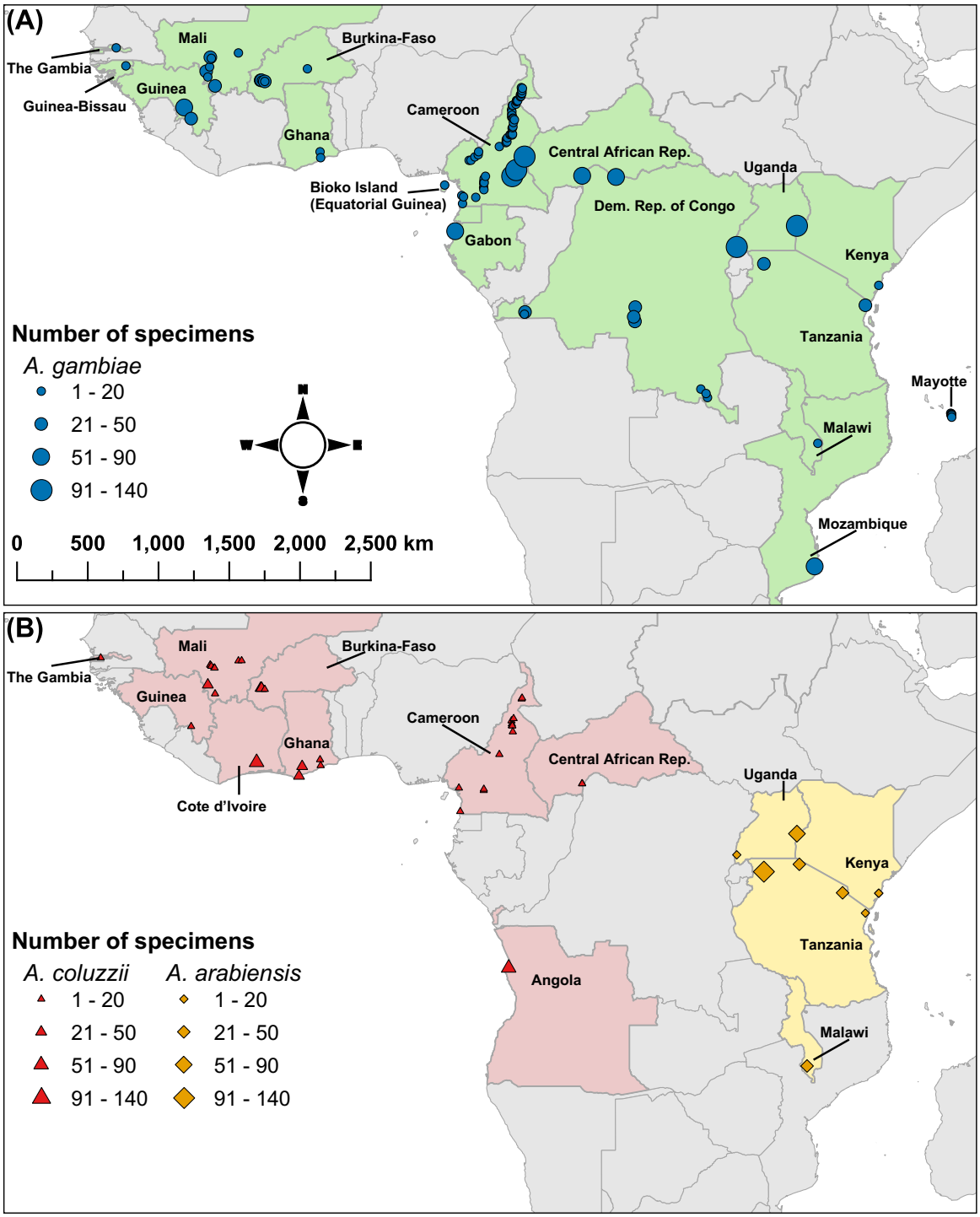

Fig. 1. Sample collection locations for (A) *A. gambiae* and (B) *A. coluzzii* and *A. arabiensis*. Symbol shape and color indicate species. Symbol size indicates the number of mosquitoes collected at the location. Green shading (A) indicates countries where *A. gambiae* were collected. Red and yellow shading (B) indicate countries where *A. coluzzii* and *A. arabiensis* were collected, respectively.

486 *A. coluzzii* (34 geolocations, 9 countries), and 359 *A. arabiensis* (8 geolocations, 4 countries). Some geolocations included samples from more than one species.

The Ag1000G data set includes genome accessibility filters that were developed by applying a machine learning model to colony crosses (https://malariagen.github.io/vector-data/ag3/methods.html). We applied these filters to exclude genomic sites where SNP calling and genotyping was less reliable. The same filter was used for the *A. gambiae* and *A. coluzzii* specimens, while a separate filter was used for *A. arabiensis*. We also excluded genomic regions with polymorphic chromosomal inversions and heterochromatic regions, as these regions of reduced recombination mask signals of geographically associated population structure in these species [25]. Within each species-level data set, we included biallelic positions with a minor allele frequency ≥ 1%, and we removed SNPs in linkage disequilibrium based on an R^2 threshold of 0.1 in moving windows of 1 kb and a step size of 1 bp. Our final data sets were based on 1,136,140 SNPs in *A. gambiae*, 1,238,862 SNPs in *A. coluzzii*, and 240,091 SNPs in *A. arabiensis*.

Genome-wide SNP frequencies reveal lower genetic differentiation between *A. gambiae* populations in West Africa and part of Central Africa than the rest of the species geographic range. We assessed population structure within this data set of *A. gambiae* WGS using PCA [28], which revealed at least nine distinct groups along the first three principal components (**Fig. 2A-B**). The first group consisted of samples from West Africa (The Gambia, Guinea-Bissau, Guinea, Mali, Burkina Faso, and Ghana) and northern Central Africa (Cameroon, Central African Republic, and the DRC province of Nord-Ubangi). *A. gambiae* from these locations showed minimal evidence

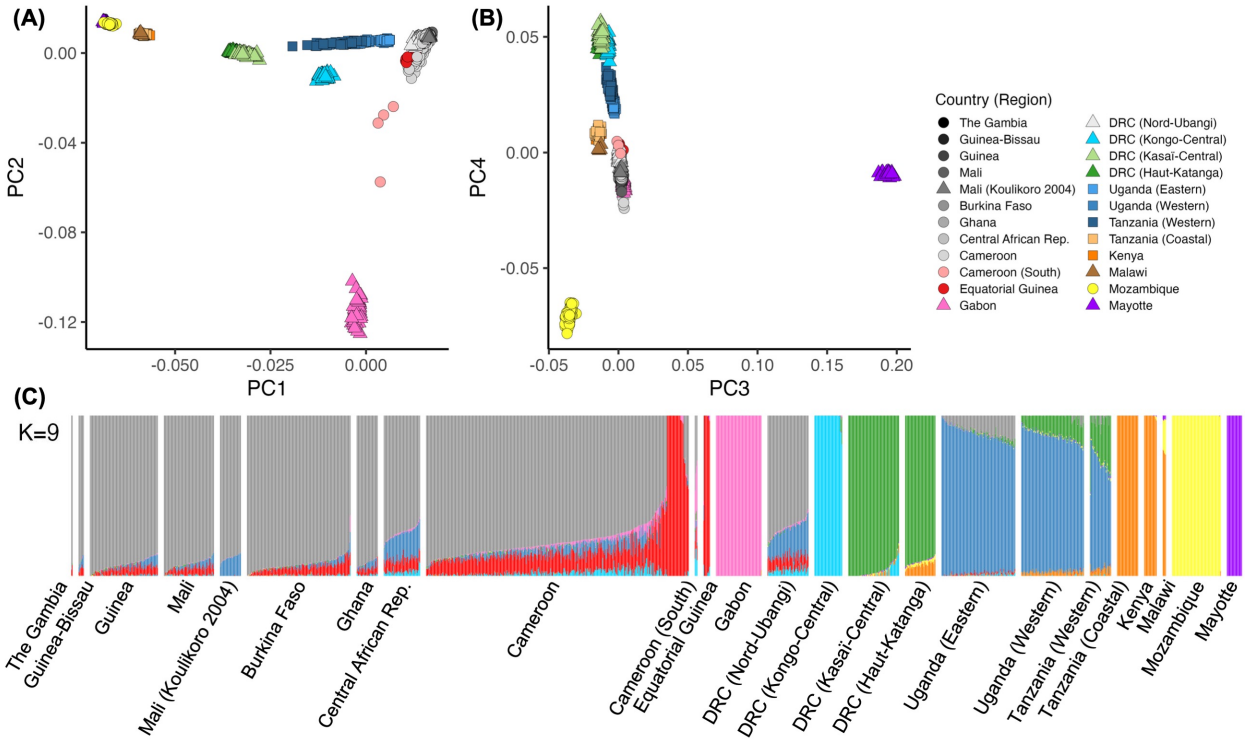

Fig. 2. Population structure of *A. gambiae*. (**A**) Principal components (PC) 1 and 2. (**B**) PCs 3 and 4. Each point within a PCA panel represents a single mosquito. Symbol color and shape indicates the country (or region within a country) where the sample was collected. (**C**) ADMIXTURE with K=9. Each bar represents an individual mosquito, with bars grouped by the country (or region within a country) where the mosquitoes were collected.

172 of spatially associated population structure within this large region. Additional clearly distinct
173 groups were formed by samples from 1) Gabon, 2) Kongo-Central Province in southwestern DRC,
174 3) Kasaï-Central and Haut-Katanga Provinces in southern DRC, 4) Uganda and western
175 Tanzania, 5) coastal Tanzania, coastal Kenya, and Malawi, 6) Mozambique, and 7) Mayotte. *A.*
176 *gambiae* from these seven regions clustered separately from each other, and from the
177 West/Central Africa group, along the first three principal components. These eight groups were
178 also apparent from the same data set using likelihood-based ADMIXTURE [29] models (**Fig. 2C**),
179 which were performed using values of K (*a priori* clusters) from 3 to 11 (**Fig. S1**). The ninth group
180 apparent from our analysis consisted of samples from Bioko Island, Equatorial Guinea. Although
181 these samples clustered with the West/Central Africa group in PCA along the first six principal
182 components, they were separated as a distinct group along PC8 (**Fig. S2**) and as a mostly distinct
183 group (together with some samples from Cameroon) in the ADMIXTURE results with K≥7 (**Fig.**
184 **2C, Fig. S1**).
185
186 The PCA and ADMIXTURE results also showed more subtle genetic differentiation within the
187 groups described above, suggesting population sub-structure within these groups of *A. gambiae*.
188 First, we observed two sub-groups within the Uganda and western Tanzania group. In the
189 ADMIXTURE results, one ancestral population contributed 43-100% of the modeled ancestry for
190 *A. gambiae* within the Uganda and western Tanzania group (**Fig. 2C**). In terms of sub-structure,
191 *A. gambiae* from eastern Uganda showed shared ancestry with the West/Central Africa group,
192 which includes Nord-Ubangi Province in northern DRC, while *A. gambiae* from western Uganda
193 and western Tanzania showed shared ancestry with Kasaï-Central and Haut-Katanga Provinces
194 in southern DRC. These results were consistent with the relative positions of these samples along
195 PC1 in the PCA results (**Fig. 2A**).
196
197 We observed additional sub-structure in East Africa between *A. gambiae* from coastal Tanzania
198 and Kenya and those from Malawi. In the ADMIXTURE results, one ancestral population
199 contributed 97-100% of the modeled ancestry for *A. gambiae* from coastal Tanzania and Kenya,
200 while *A. gambiae* from Malawi showed shared ancestry (19-22%) with those from Mozambique
201 (**Fig. 2C**). In the PCA results, *A. gambiae* from Malawi separated as a distinct group along PC6
202 (**Fig. S2**).
203
204 Within Cameroon the strongest evidence for population sub-structure was between *A. gambiae*
205 from South Region and those from the remaining administrative regions of the country, although
206 our interpretation is limited by the number of specimens from South Region (n = 4). In the PCA
207 results, these individuals from South Region appeared between *A. gambiae* from the remaining
208 locations in Cameroon and those from Gabon along PC2 (**Fig. 2A**), and in the ADMIXURE results
209 the individuals from South Region appeared to share an equal amount of ancestry between those
210 same two groups (**Fig. 2C**). While we also observed some additional evidence of population
211 structure within Cameroon, e.g., along PC5 and PC10 (**Fig. S2**) and with ADMIXTURE from K≥7
212 (**Fig. S1**), these differentiated specimens were not clustered geographically.
213
214 Within the West/Central Africa group, the ADMIXTURE model indicated that most *A. gambiae*
215 shared common ancestry with the Uganda and western Tanzania group for a small proportion of
216 their genome (**Fig. 2C**). Notably, there was an east-to-west gradient in the proportion of ancestry
217 attributed to this group, with samples from Guinea, Mali, Burkina Faso and Ghana showing lower
218 proportions than those from Central African Republic and Nord-Ubangi Province in northern DRC.
219 Additionally, *A. gambiae* collected in 2004 from Koulikoro Region, Mali (n = 32) showed subtle,
220 but still mostly distinct, genetic differentiation from the remaining *A. gambiae* collected in West

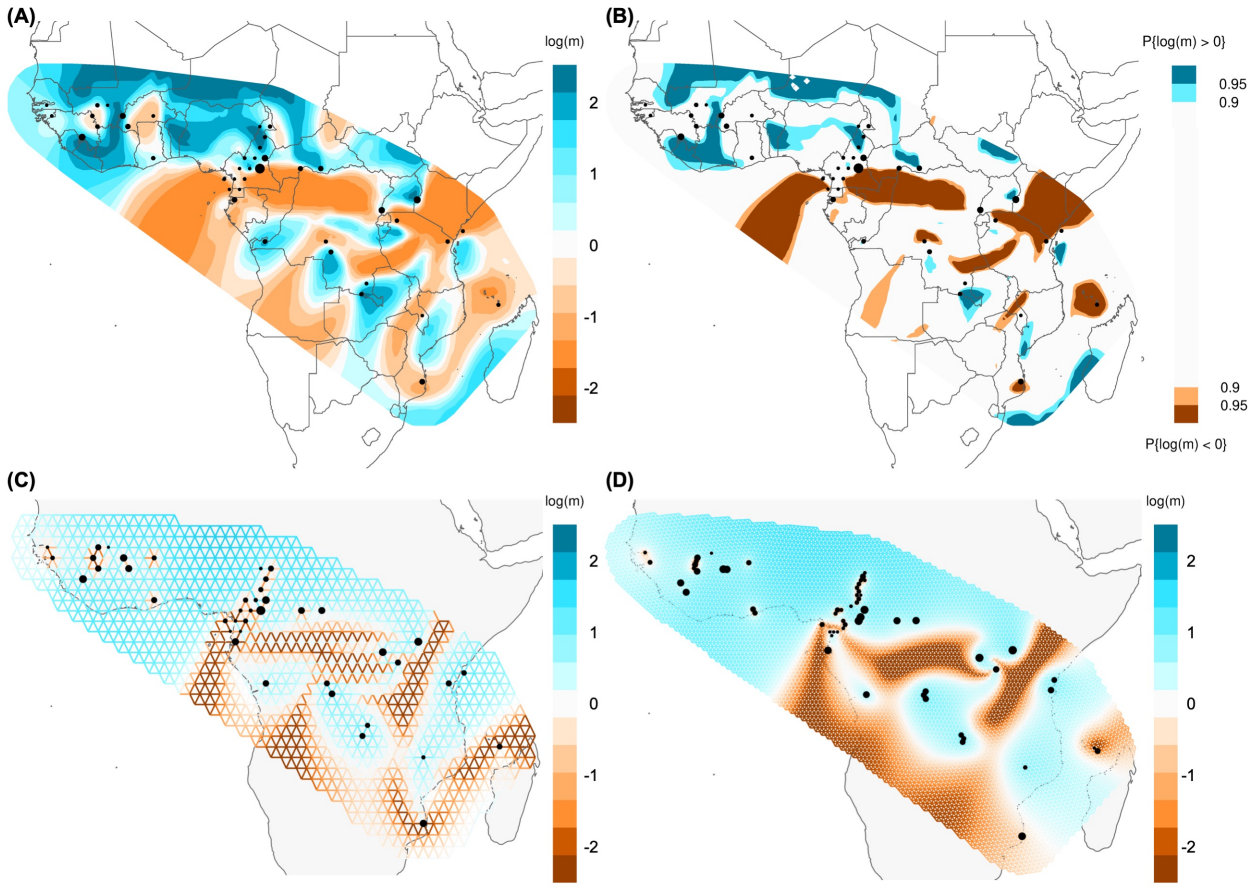

Fig. 3. Estimated effective migration surfaces for *A. gambiae*. (**A**) Posterior mean effective migration rates, log10(*m*), from EEMS. (**B**) Posterior probabilities of the effective migration rate, log10(*m*), being greater than or less than 0 from EEMS. (**C**) Effective migration rates, log10(*m*), from FEEMS using the same grid resolution as panel **A**. (**D**) Effective migration rates, log10(*m*), from FEEMS using a higher resolution grid, with edge lengths of 55 km. Black circles show the geolocations of samples included in the analysis, aligned to the nearest node on the grid, with circle size scaled to the number of samples.

Africa according to ADMIXTURE (**Fig. 2C** and **Fig. S1**) as well as PCA along PC9 (**Fig. S2**). Nearby collections included specimens from Segou Region, Mali (n = 1) and Centre-Sud Region, Burkina Faso (n = 13) in 2004, and specimens from Mali, Guinea and Burkina Faso in 2012 and 2014, including 33 specimens from Koulikoro Region, Mali, all of which were more similar to each other than the Koulikoro 2004 specimens. Potential explanations for these subtle differences include genetic changes over time in *A. gambiae* populations in Koulikoro, or long-distance migration [30] from an unsampled location to Koulikoro. However, the available data are not sufficient to distinguish between these or other hypotheses.

<u>Migration rates between *A. gambiae* populations vary across the species geographic range</u>

We used EEMS to create maps of effective migration rates for *A. gambiae*, thereby visualizing where the genetic differentiation between the populations of *A. gambiae* described above was higher or lower than expected based on the geographic distance between the sampling locations. The null model in EEMS is that any observed differentiation between populations is the result of isolation-by-distance, and the mean rate of increase in differentiation across all populations determines the mean migration rate across the geographic range being mapped. The effective migration rates (*m*) modeled by EEMS are parameterized as deviations from this mean rate (μ),

so that $\log_{10}(m) = 0$ is equivalent to the overall mean rate, and $\log_{10}(m) = 1$, for example, corresponds to effective migration at a rate ten times higher than the overall mean [13]. We found that the genetic differentiation among *A. gambiae* from locations in the West/Central Africa group described above was generally much less than would be expected under isolation-by-distance (**Fig. 3**). Consequently, the effective migration rates between locations in this region estimated by EEMS were generally higher than, or at least equal to, the mean rate across all sampled locations. In addition to the map visualizing the point estimates of $\log_{10}(m)$ across space (**Fig. 3A**), the EEMS model also maps exceedance probabilities, showing where the posterior probability of the $\log_{10}(m)$ being greater than or less than 0 exceeds 0.90 or 0.95 (**Fig. 3B**). This latter map provides a visualization of where migration rates are most likely to depart from the overall mean rate of $\log_{10}(m) = 0$, thereby indicating regions with the highest confidence migration barriers or corridors based on the EEMS model. For example, there are several areas within the West/Central Africa group of *A. gambiae* where the probability of a higher than expected migration rate is greater than 0.90, while there are none with this high probability of a lower than expected migration rate.

Outside of the West/Central Africa group, we found that the genetic differentiation between *A. gambiae* from the other populations described above was generally higher than expected under isolation-by-distance, resulting in lower-than-average effective migration rates estimated by EEMS. These lower-than-average migration rates indicate the presence of barriers to migration and/or absence of facilitators of migration for *A. gambiae* moving between these regions. For example, EEMS estimated lower than average migration rates for *A. gambiae* across the Rift Valley Complex in East Africa, between northern and southern areas of Central Africa, and between Bioko Island and Cameroon. This last example highlights additional insights possible from spatially explicit analyses such as EEMS. While the results from PCA and ADMIXTURE indicated relatively subtle genetic differentiation between *A. gambiae* from Bioko Island and Cameroon, the results from EEMS indicate that those differences were higher than expected under isolation-by-distance, presumably due to the roughly 30 km of ocean acting as a barrier to migration between Bioko Island and the mainland. A second example is that the effective migration rates between the West/Central Africa group and eastern Uganda were likely equal to, or slightly higher than, the mean rate expected under isolation-by-distance. Although the PCA and ADMIXTURE results showed distinct genetic differentiation between *A. gambiae* from the West/Central Africa group and those from eastern Uganda, the results from EEMS (**Fig. 3A-B**) indicated that these differences may be due to isolation-by-distance.

<u>Migration rate estimates were robust to changes in grid size and jackknife resampling</u>

We investigated the robustness of our estimated effective migration rate maps in several ways using Fast Estimation of Effective Migration Surfaces (FEEMS), a method that is conceptually similar to EEMS but which uses a penalized likelihood framework to allow more efficient optimization and output [14]. One limitation of EEMS is that it is computationally intensive, whereas the higher computational efficiency of FEEMS allows for estimation of effective migration rate maps at high throughput and with much finer geospatial resolution. In both EEMS and FEEMS, estimates of migration rates are made along a triangular grid, where grid vertices represent demes in a stepping-stone model, and each sampling location is assigned to the nearest vertex on the grid.

First, we compared the outputs of EEMS and FEEMS by running both models using the same 1000-deme grids, which is the finest resolution possible with EEMS. The effective migration surfaces estimated by EEMS (**Fig. 3A**) and FEEMS (**Fig. 3C**) for *An. gambiae* were generally similar, especially in areas nearest to the geolocations where samples were collected. Both

methods estimated lower than average migration rates for *A. gambiae* across the Great Rift Valley in East Africa, between northern and southern areas of Central Africa, and between Bioko Island and Cameroon; as well as higher than average migration rates across most of West Africa. Although there were also areas where the estimates of effective migration for *A. gambiae* differed between the two methods, these differences generally occurred where the exceedance probability map from EEMS (**Fig. 3B**) indicated lower confidence that the estimates were different from 0 (i.e., $P(\log(m) \neq 0) < 0.90$).

To assess the effect of grid resolution on model outcomes [31], with more vertices (demes) than possible in EEMS, we ran FEEMS using a range of grid resolutions, with edge lengths of 55, 110 and 220 km for each species. The 220 km edges corresponded with the finest resolution possible in EEMS, while each halving of the edge length increased the number of grid nodes by approximately four-fold. The results from FEEMS were robust to changes in the grid resolution when comparing across edge sizes from 55 km to 220 km (**Fig. 3C-D, Fig. S3-S5**), with both high and low migration estimates occurring in the same regions across all three grids. Notably, the FEEMS results were more dependent on the smoothing parameter, lambda, than on the grid resolution (**Fig. S3-S5**). In the main text (**Fig. 3C-D**), we have presented results from FEEMS using the value for that had the lowest mean square cross-validation error across a range of lambda from 0.1 to 100 (**Fig. S3-S5**).

Finally, we visually assessed the resulting maps from each iteration of jackknife cross-validation to assess the robustness of FEEMS estimates to removal of observed specimens from a single deme (**Supplementary file Ag FEEMS jackknife maps**). In general, removing a single observed

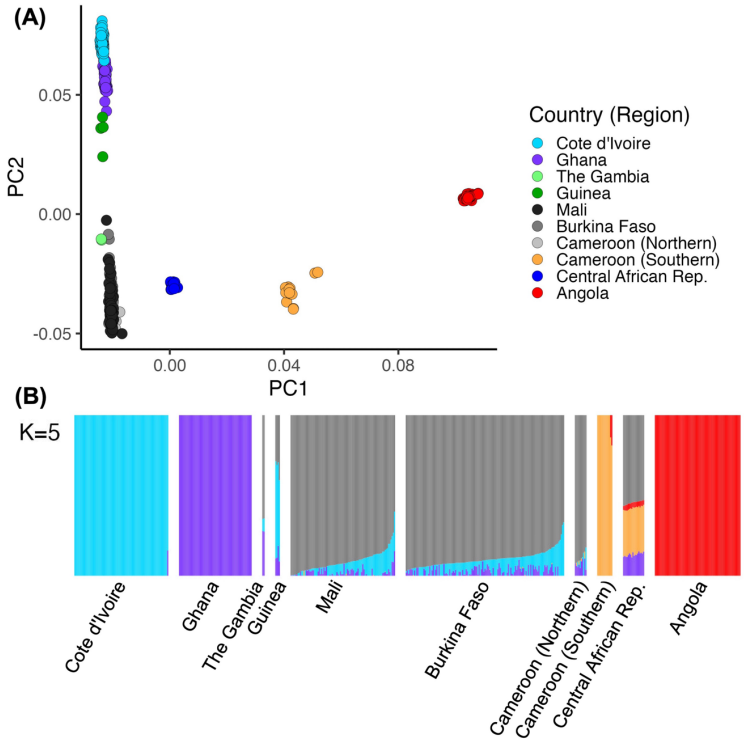

Fig. 4. Population structure of *A. coluzzii*. (**A**) Principal components (PC) 1 and 2. Each point represents a single mosquito. Symbol color indicates the country (or region within a country) where the sample was collected. (**B**) ADMIXTURE with K=5. Each bar represents an individual mosquito, with bars grouped by the country (or region within a country) where the mosquitoes were collected.

deme from the FEEMS model had a greater influence on the surrounding migration rate estimates for demes with fewer nearby neighboring observed demes. In other words, migration rates estimated by FEEMS were generally robust to the removal of data from a single location when data were available for other nearby locations. One exception to this result was the influence of the *A. gambiae* specimens collected near Koulikoro, Mali, in 2004. In this case, the genetic differentiation between these specimens and those from several nearby locations caused FEEMS to estimate relatively low migration rates near Koulikoro. When the Koulikoro specimens were removed, the FEEMS model estimated relatively high migration rates in this region. As with the PCA and ADMIXTURE results, potential explanations for the different estimates of effective migration rates here include genetic changes over time in *A. gambiae* populations in Koulikoro, or long-distance migration [30] from an unsampled location to Koulikoro.

Anopheles coluzzii in West and Central Africa had higher genetic differentiation between populations than *A. gambiae* in the same region

The spatial extent of locations where the *A. coluzzii* were collected included most of the West/Central Africa region where *A. gambiae* showed very little spatially associated population structure. Over that same region, we found distinct genetic differentiation between *A. coluzzii* from different locations according to the results of PCA (**Fig. 4A**) and ADMIXTURE (**Fig. 4B**). In some cases, e.g. between coastal and inland populations, those differences were greater than would be expected under isolation-by-distance, according to our analysis using EEMS (**Fig. 5**).

Four broader geographic groups of *A. coluzzii* were apparent: 1) locations nearer to the coast of West Africa in Ghana and Côte d'Ivoire; 2) locations nearer to the Sahel region of West and Central Africa, including Mali, Burkina Faso and three northern regions of Cameroon (Far North, North, and Adamawa); 3) three southern regions of Cameroon (Centre, Littoral, and South); and 4) Angola. In addition to these broader groups, *A. coluzzii* from Guinea and Central African Republic provide two examples of populations that may be admixtures of separate ancestral populations. First, *A. coluzzii* from Guinea clustered between the coastal West Africa and Sahelian individuals in PCA (**Fig. 4A**), while the ADMIXTURE results showed *A. coluzzii* from Guinea sharing genetic patterns of both regions for K values from 3 to 8 (**Fig. 4B** and **Fig. S6**). Second, *A. coluzzii* from Central African Republic formed a distinct cluster in the PCA plots,

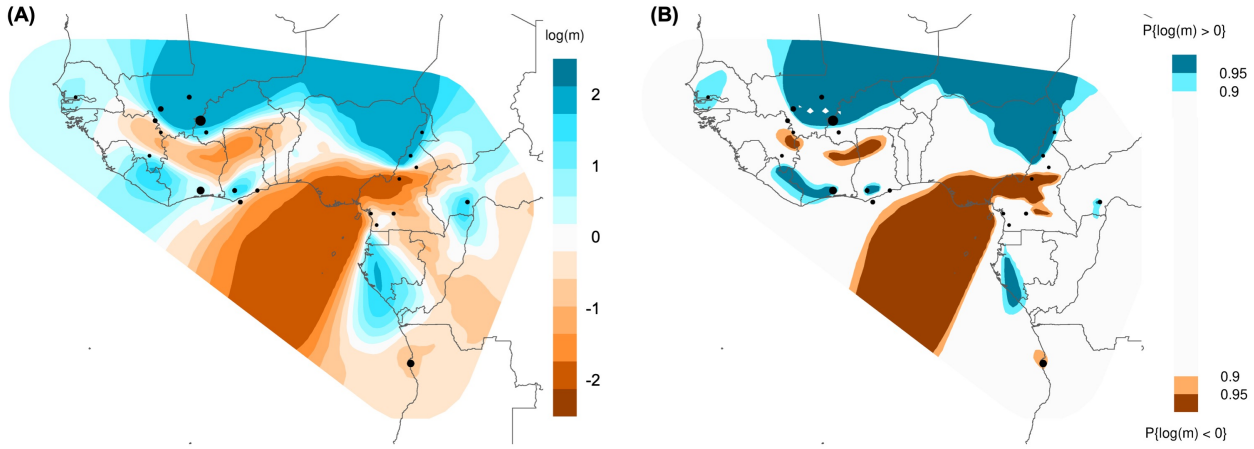

Fig. 5. Estimated effective migration surfaces for *A. coluzzii*. (**A**) Posterior mean effective migration rates, $\log_{10}(m)$, from EEMS. (**B**) Posterior probabilities of the effective migration rate, $\log_{10}(m)$, being greater than or less than 0 from EEMS. Black circles show the geolocations of samples included in the analysis, aligned to the nearest node on the grid, with circle size scaled to the number of samples.

clustering between individuals from southern Cameroon and individuals from northern Cameroon along PC1 (**Fig. 4A**), and they showed ancestry matching both southern and northern Cameroon in the ADMIXTURE results for values of K from 2 to 5 (**Fig. 4B** and **Fig. S6**).

We found the highest estimated effective migration rates among *A. coluzzii* from locations near the Sahel (Mali, Burkina Faso and northern Cameroon), based on results from EEMS (**Fig. 5**) and FEEMS (**Fig. S7-S10**). For *A. coluzzii* from Ghana and Côte d'Ivoire, the effective migration rates between these geolocations estimated by EEMS were higher than average, indicating that the subtle genetic differences between samples from these two countries, observed in PCA and ADMIXTURE, were less than expected given the geographic distance. The lowest estimated effective migration rates were observed between the geographic groupings outlined above. Notably, these estimates were relatively close to the mean migration rate in some cases, for example between *A. coluzzii* from southern Cameroon and Angola (**Fig. 5**). Given the long distance between those two locations, this indicates that the clear genetic differentiation between the respective populations is approximately as much as would be expected under uniform isolation-by-distance.

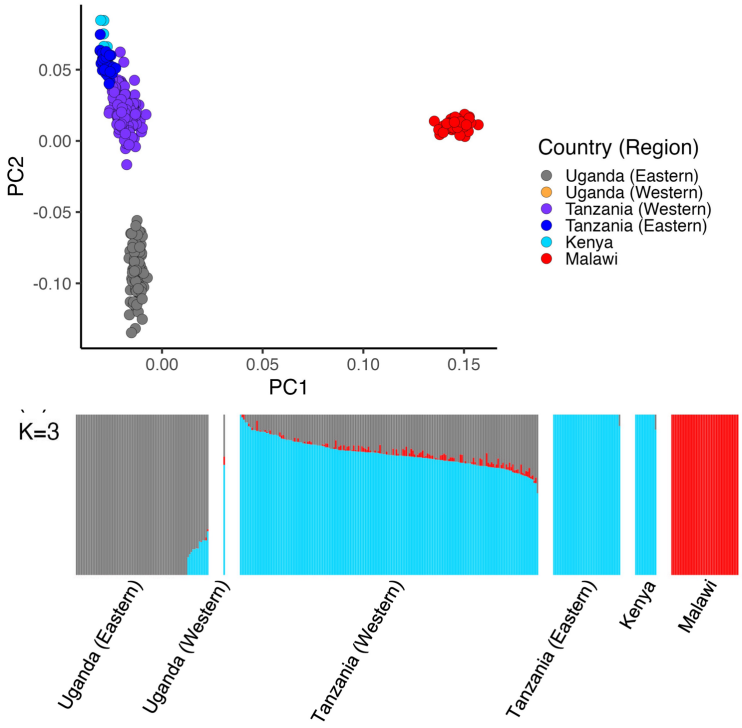

Fig. 6. Population structure of *A. arabiensis*. (**A**) Principal components (PC) 1 and 2. Each point represents a single mosquito. Symbol color indicates the country (or region within a country) where the sample was collected. (**B**) ADMIXTURE with K=5. Each bar represents an individual mosquito, with bars grouped by the country (or region within a country) where the mosquitoes were collected.

<u>*Anopheles arabiensis* in East Africa had lower genetic differentiation between populations than *A. gambiae* in the same region</u>

The data set analyzed here included fewer specimens of *A. arabiensis* (n = 359) from fewer unique sampling locations (eight) than the other two species, and the locations covered only a

portion of the known species range of *A. arabiensis*. Still, the sampling locations mostly overlapped with those of *A. gambiae* in East Africa, providing an opportunity for comparisons between these two species. We observed distinct genetic differentiation between *A. arabiensis* from three geographic groupings: 1) Malawi; 2) eastern Uganda; and 3) Kenya and Tanzania (**Fig. 6**). Additionally, the geolocation in western Uganda, which only had one specimen of *A. arabiensis*, grouped with *A. arabiensis* from Kenya and Tanzania. The results from EEMS (**Fig. 7A**) and FEEMS (**Fig. S12-S15**) suggest similar groupings, with *A. arabiensis* from Malawi and eastern Uganda separated from the other regions by areas of low migration rates. However, the exceedance probability map from EEMS (**Fig. 7B**) shows less than 90% probability across most of the study area that the migration rates differ from the mean rate expected by isolation-by-distance, possibly due to the low number of specimens and locations in this data set.

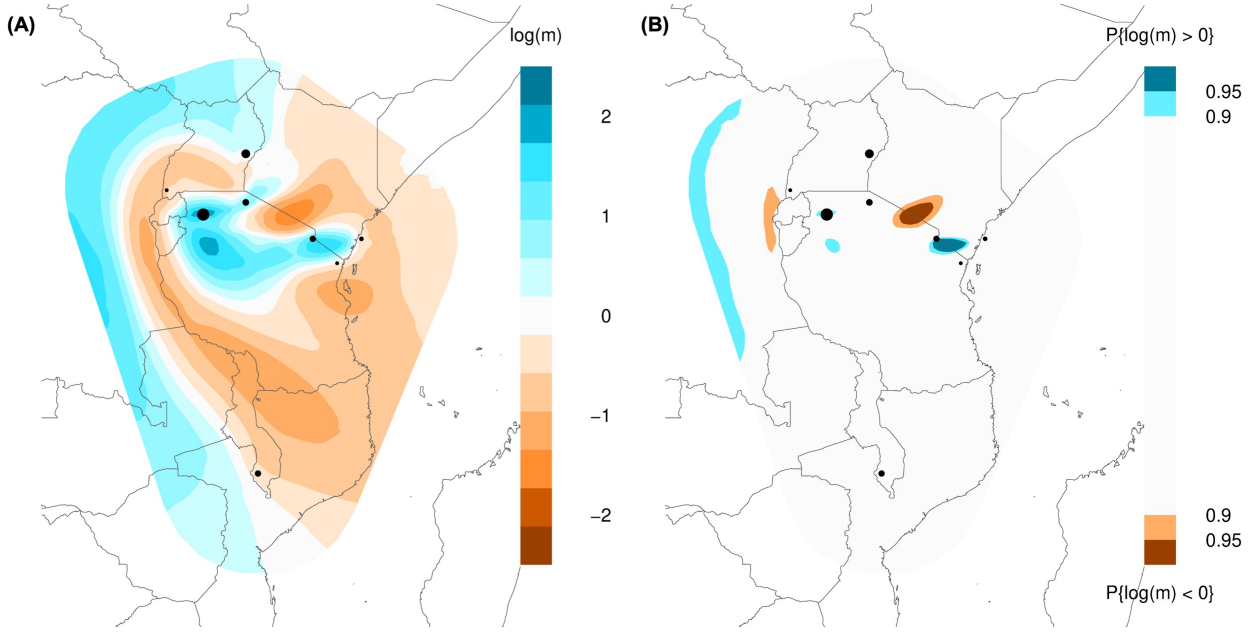

Fig. 7. Estimated effective migration surfaces for *A. arabiensis*. (**A**) Posterior mean effective migration rates, $\log_{10}(m)$, from EEMS. (**B**) Posterior probabilities of the effective migration rate, $\log_{10}(m)$, being greater than or less than 0 from EEMS. Black circles show the geolocations of samples included in the analysis, aligned to the nearest node on the grid, with circle size scaled to the number of samples.

Within the Kenya and Tanzania group, there was some evidence of additional sub-structure, but it was relatively subtle. *A. arabiensis* from western Tanzania (Muleba/Kagera and Tarime/Mara) formed a cluster along PC2, which mostly does not overlap with *A. arabiensis* from eastern Tanzania (Moshi/Manyara and Muheza/Tanga) and Kenya (Kilifi). The ADMIXTURE results show a similarly subtle difference between *A. arabiensis* from these regions (**Fig. 6B** and **Fig. S11**). This same pattern is apparent in the results from EEMS, with an area of lower effective migration estimated in northern Tanzania between samples from Tarime (to the west) and Moshi (to the east; **Fig. 7**). However, according to the FEEMS results (**Fig. S12-S15**), the genetic differentiation between samples from Moshi in eastern Tanzania and Muleba and Tarime in western Tanzania was less than expected under isolation-by-distance (i.e., high estimated effective migration), while the genetic differentiation between samples from Moshi and coastal Tanzania and Kenya were greater than expected based on the geographic distance (i.e., low estimated effective migration).

Discussion

In this study, we assessed the population structure of three African malaria vector species and estimated effective migration rates between populations within each species. We found that the genetic differentiation observed between populations of *A. gambiae* from East, Southern and part of Central Africa was greater than would be expected under uniform isolation-by-distance, with relatively low effective migration rates estimated between populations in these regions. These results contrast with our observations of *A. gambiae* populations in West and northern Central Africa, which had low genetic differentiation despite the long geographic distances between them, corresponding with relatively high effective migration rates in these regions. In contrast to *A. gambiae*, we found greater genetic differentiation between *A. coluzzii* populations in West and Central Africa, indicating that these closely related species respond to, or interact with, barriers and/or facilitators of migration in this region differently. Conversely, we found less distinct population structure between *A. arabiensis* specimens from East Africa, especially within Tanzania, compared to *A. gambiae*. These results demonstrate that migration rates between populations vary across geographic distributions of these important malaria vectors, likely in response to ecological barriers or facilitators of migration. Furthermore, these apparent effects on migration differ between species, even for very closely related species.

This is the first study to use the EEMS framework [13, 14] to elucidate the spatial population structure of a disease vector. While PCA and ADMIXTURE allowed us to visualize the relative genomic similarity of the sampled vectors and thereby identify groups of sampling locations with higher genetic similarity compared to the other groups, PCA and ADMIXTURE do not account for the geographic distances between sample collection sites. By using EEMS to explicitly model both the genomic data and the sampling locations, we were able to visualize how migration rates likely vary across the landscape to produce the observed patterns of relative genetic differentiation among the sampled geolocations. While each of these methods has its own strengths and weaknesses, we have focused here on findings that were consistent across the methods, for which we have the highest confidence. Additionally, we have highlighted findings from EEMS that differ from the PCA and ADMIXTURE results when these were plausibly explained by the geographic distances between sample collection sites.

This study expands on previous assessments of population structure in the *A. gambiae* species complex based on earlier phases of the Ag1000G project [25, 26]. Those studies found low genetic differentiation between *A. gambiae* from West Africa (Guinea, Burkina Faso, and Ghana), Cameroon and Uganda; and they showed greater genetic differentiation between samples from Bioko Island (Equatorial Guinea), Gabon, Mayotte, and Coastal Kenya, and between each of those locations and West/Central Africa. With the addition of *A. gambiae* specimens from Mali, Central African Republic, Democratic Republic of Congo, Tanzania, Malawi, and Mozambique, our updated analyses largely align with the previous findings: *A. gambiae* across West and northern Central Africa show very little genetic differentiation, while samples from locations outside this region show more distinct genetic differentiation. Our results here differ slightly from the previous findings, in that we found distinct genetic differentiation between *A. gambiae* from Uganda and the West/Central Africa group. However, this genetic differentiation was less than we observed between other populations, and our EEMS and FEEMS analyses suggest that migration between populations of *A. gambiae* in Uganda and Central Africa (e.g. northern DRC, Central African Republic and Cameroon) may be occurring at roughly the rate expected under isolation-by-distance, or even slightly higher. Ultimately, denser mosquito sampling is needed to better delineate the population structure of *A. gambiae* across the geographic distribution of this malaria vector species. As the availability of *A. gambiae* genomic sequences from previously

437 unrepresented regions continues to increase, we expect additional geographically associated
438 population structure to be revealed.
439
440 Phase 2 of the Ag1000G project [26] showed differentiation between *A. coluzzii* specimens from
441 coastal West Africa (Ghana and Côte d'Ivoire) and further inland (Burkina Faso). With the addition
442 of specimens from Mali and Cameroon in the phase 3 data set, our analyses suggest a broader
443 pattern: *A. coluzzii* nearer to the Sahel region of West and Central Africa (Mali, Burkina Faso and
444 northern Cameroon) show very little genetic differentiation from each other but show distinct
445 genetic differentiation from *A. coluzzii* nearer to the coast (Ghana, Côte d'Ivoire and southern
446 Cameroon). While the high effective migration rates estimated here for *A. coluzzii* from the near-
447 Sahel region are consistent with the estimates for *A. gambiae* in the same region, we found
448 differences between the two species in the way these near-Sahel populations are connected, or
449 not, to coastal populations, with *A. coluzzii* having lower effective migration rates between the
450 coast and inland, and *A. gambiae* being more connected. These differences in population
451 connectivity between two closely related species in the same region suggest that different factors
452 may either impede or facilitate successful migration in each species. Potential factors could
453 include long-distance windborne dispersal [30] or adaptations to local habitats [32]. One limitation
454 of this comparison between species was that the number of specimens, and the number and
455 location of sampling sites, differed between species. Still, there was considerable spatial overlap,
456 with both *A. gambiae* and *A. coluzzii* collected from 28 of the 34 sites with *A. coluzzii*.
457
458 This is the first study to look at the population structure of *A. arabiensis* using whole-genome
459 sequences. The Ag1000G project phase 3 data set used in this study includes samples from East
460 and Southern Africa, and our results are broadly consistent with previous studies of *A. arabiensis*
461 population structure in this region based on microsatellites. Donnelly and Townson [33] covered
462 a relatively broad spatial scale, assessing samples of *A. arabiensis* from nine locations in five
463 countries, from Sudan in the north to Mozambique in the south, and found five groupings of sub-
464 populations that each aligned with the country where the samples were collected. These results
465 showed evidence of population structure at a broad spatial scale across the region, consistent
466 with our study. At a finer scale, Maliti *et al.* [34] assessed *A. arabiensis* and *A. gambiae* in central,
467 coastal and island regions of Tanzania, and they found less population structure in *A. arabiensis*
468 in this area than for *A. gambiae*. Similarly, Kamau *et al.* [35] found genetic differentiation between
469 samples of *A. gambiae* in western and coastal Kenya, but not *A. arabiensis*. Our finding of less
470 distinct population structure between samples of *A. arabiensis* from East Africa, compared to *A.*
471 *gambiae*, is consistent with these previous studies, despite the limited scope of our *A. arabiensis*
472 data set.
473
474 Our analyses were based on a large number of biallelic SNPs with a minor allele frequency ≥ 1%
475 (> 1 million SNPs in *A. gambiae* and *A. coluzzii*, and > 200,000 SNPs in *A. arabiensis*). The signal
476 from analyses of population structure from this type of data is likely driven by migration over
477 several generations stretching to the relatively distant past due to reasons including: (1) the
478 relatively old ages of common neutral variants [36], and (2) the use of SNP-based genetic distance
479 metrics that capture mean coalescent times over a long history instead of the frequencies of
480 recent coalescent events [37]. Future analyses using metrics capable of capturing more recent
481 information, such as rare variants with younger ages [38] or longer shared segments of the
482 genome that are identical-by-descent and that reflect more recent recombination and coalescent
483 events [37, 39-42], could provide more insights into recent gene flow.
484

485 In conclusion, our results, supported by those of several previous studies, establish that migration
486 rates between malaria vector populations vary both between and within species, presumably
487 based on species-specific responses to ecological or environmental conditions that may impede
488 or facilitate migration, and the geographical patterns of these conditions across the landscape.
489 These differences within and between species have potential implications for malaria research
490 and control programs planning surveillance of vector populations, monitoring for insecticide
491 resistance, and evaluating interventions. These findings should also be considered when planning
492 multi-country malaria control strategies, e.g. the Elimination Eight initiative [43], or developing
493 novel control strategies that rely on mosquito mating, e.g. genetic modification [18]. These
494 findings also raise questions about which environmental features may be acting as migration
495 barriers or corridors for malaria vectors, and whether these features may change over time.
496
497 **Methods**
498 Whole genome sequencing and SNP calling
499 Whole genomes of 4,693 individual mosquitoes were sequenced at the Wellcome Sanger Institute
500 for the Ag1000G phase 3 data set. Sequencing was done on the Illumina HiSeq 2000 platform
501 (100 bp paired-end reads) or Illumina HiSeq X platform (150 bp paired-end reads). Sequence
502 reads were aligned to the AgamP4 reference genome using BWA version 0.7.15. Indel
503 realignment and SNP calling were done using GATK version 3.7-0. Mosquitoes were excluded if
504 median coverage across all genome positions (across all chromosomes) was less than 10x, or if
505 less than 50% of the reference genome was covered by at least 1x. Additional mosquitoes were
506 excluded based on analyses to identify cross-contamination and population outliers. More details
507 about the Ag1000G project, including descriptions of the partner studies and quality assessment
508 and quality filtration steps for the whole-genome sequence data are available at
509 https://malariagen.github.io/vector-data/ag3/ag3.0.html. The final Ag1000G phase 3 data set
510 included 2,784 mosquitoes collected from natural populations in 19 countries.
511
512 We also included 165 additional *A. gambiae* from 8 locations in Democratic Republic of Congo
513 and 5 additional *A. gambiae* from 1 location in Malawi. The 165 specimens from Democratic
514 Republic of Congo were sequenced at Wellcome Sanger Institute on an Illumina HiSeq (150 bp
515 paired-end reads) as part of the Vector Observatory project under sample set ID 1264-VO-CD-
516 WATSENGA-VMF00164 as described in Dennis *et al*. [44]. The 5 *A. gambiae* from Malawi were
517 sequenced at the University of Marland on the Illumina NovaSeq 6000 platform (150 bp paired-
518 end reads). Sequence alignment, indel realignment, SNP calling, and all quality assessment and
519 filtration steps for these 170 specimens were performed following the same steps as used for the
520 Ag1000G phase 3 data set.
521
522 Included samples and genomic positions
523 Analyses described here were done separately for each species. Specimens were assigned to
524 each species according to a principal components analysis (PCA) described in more detail at
525 https://malariagen.github.io/vector-data/ag3/methods.html. Specimens assigned to a cryptic
526 taxon and those that appeared to be F1 hybrids were excluded from this study.
527
528 Genome accessibility filters were developed by applying a machine learning model to colony
529 crosses (https://malariagen.github.io/vector-data/ag3/methods.html), and these filters were
530 applied to exclude genomic sites where SNP calling and genotyping was less reliable. The same
531 filter was used for *A. gambiae* and *A. coluzzii*, while a separate filter was used for *A. arabiensis*.
532

Pairwise kinship coefficients were estimated using KING version 2.2.7 to identify first-degree relatives (full siblings or parent-offspring). These kinship analyses were based on the euchromatic regions of the autosomal chromosomes, using only biallelic positions with a minor allele frequency ≥ 1%. After identifying all first-degree relative pairs, kin-groups were constructed such that each group contained all first-degree relatives from the data set for all individuals in the kin-group. All but one mosquito from each kin-group were excluded from further analysis, leaving 1,565 *A. gambiae*, 486 *A. coluzzii*, and 359 *A. arabiensis*.

For all subsequent analyses, we excluded genomic regions with polymorphic chromosomal inversions in addition to excluding heterochromatic regions. For *A. gambiae* and *A. coluzzii*, we used genomic positions on chromosome 3R from 1-37 Mb and on chromosome 3L from 15-41 Mb. Due to an additional inversion polymorphism on chromosome 3R in *A. arabiensis*, we only included chromosome 3L (15-41 Mb) in that species. Within each species-level data set, we only included biallelic positions with a minor allele frequency ≥ 1%, and we removed SNPs in linkage disequilibrium based on an R^2 threshold of 0.1 in moving windows of 1 kb and a step size of 1 bp.

Spatial data

The geolocation for each sampled mosquito was recorded as part of each contributing study to the Ag1000G project (https://malariagen.github.io/vector-data/studies-ag1000g.html). Sampling locations for the 165 *A. gambiae* collected in Democratic Republic of Congo (sample set ID 1264-VO-CD-WATSENGA-VMF00164) are described by Dennis *et al.* [44]. The five *A. gambiae* from Malawi were collected as blood-fed adult females from inside houses near Ntaja Health Center in Machinga District, Malawi, in March-April 2022. In most contributing studies, all mosquitoes sampled from the same village were assigned the same GPS coordinates, i.e., for that village, such that the coordinates are accurate to within a few hundred meters, at worst. For 5 out of 128 unique geolocations, all mosquitoes from the same county or district were assigned to the same GPS coordinates, such that those coordinates are only accurate to within ~20-50 km. Notably, for those 5 sample geolocations, the next nearest neighbor was ~200-800 km away, and therefore the GPS coordinates were sufficiently accurate for our analyses.

For generation of estimated effective migration surfaces (EEMS and FEEMS), the geographic boundary of each map was defined as a convex hull 600 km beyond the outermost geolocations in each sample set to reduce potential edge effects.

Population structure

PCA was performed using PLINK version 1.90b6.18. Within each species, we plotted the principal components with the highest eigenvalues (explaining the highest percentage of the variance) after examining the scree plot. For all PCA plots, individual samples were color-coded by country (or administrative regions when applicable) to visually assess potential associations between genetic clustering and sample geolocations.

Admixture models were performed using ADMIXTURE version 1.3.0 for values of K (clusters) from 3 to 11 (*A. gambiae*), 2 to 8 (*A. coluzzii*) and 1 to 5 (*A. arabiensis*), with the range of K based on assessment of PCA results. For each value of K within each species, we ran ten replicates of ADMIXTURE, each with a different random seed, and conducted 5-fold cross validation on each replicate. We set the point estimation algorithm to stop when the log-likelihood increased by less than $\varepsilon = 10^{-4}$ between iterations (the default). Within each value of K, we plotted the run with the highest likelihood, grouping samples by country (or administrative regions where applicable) to visually assess potential associations between genetic clustering and sample geolocations.

582
583 Estimating effective migration surfaces
584 Effective migration surfaces were estimated using EEMS [13] and FEEMS [14]. Both models
585 estimate effective migration over a geographic area by comparing genetic similarity and
586 geographic distance among sampled geolocations in the area of interest. In both analyses,
587 estimates are made along a triangular grid, with each sampling location assigned to the nearest
588 vertex on the grid. The grid vertices represent demes in a stepping-stone model, whereby each
589 deme exchanges migrants only with its neighbors (i.e. along the edges connecting the vertices).
590 In cases with equal migration rates between all demes, this produces the null model of isolation-
591 by-distance. Both methods parameterize the effective migration rates (m) as deviations from an
592 overall mean rate (μ) across the entire area of interest, so that $\log_{10}(m) = 0$ is equivalent to the
593 overall mean rate, and $\log_{10}(m) = 1$ corresponds to effective migration at a rate ten times higher
594 than the overall mean [13].
595
596 Effective migration rates in EEMS are estimated using vertex-based Voronoi tessellations, with
597 model parameters fit by MCMC [13]. We used 18 million MCMC iterations with 14 million iterations
598 of burn in for *A. gambiae*, 14 million iterations (10 million burn in) for *A. coluzzii*, and 6 million
599 iterations (2 million burn in) for *A. arabiensis*. The number of iterations was based on observed
600 convergence and accepted parameter distributions (following recommendations in the EEMS
601 documentation) across 10 independent chains per species. For all three species, we thinned the
602 MCMC every 9,999 iterations and set the EEMS grid resolution to the maximum number of demes
603 allowed by the software (1000 demes). For *A. gambiae*, the first 10 independent MCMC chains
604 found separate local optima. We subsequently ran 20 additional independent chains and selected
605 the 10 chains with the highest log-likelihoods (of the 30 chains that were run) to produce the final
606 EEMS output shown in the figures.
607
608 Two types of maps are used to display the outputs from EEMS across the area of interest. One
609 shows the posterior means of the effective migration rates, $\log_{10}(m)$. The other map shows
610 exceedance probabilities – in this case, showing where the posterior probability of the $\log_{10}(m)$
611 being greater than or less than 0 exceeds 0.90 or 0.95. While the former provides a visualization
612 of the point estimates of $\log_{10}(m)$ across space, the latter provides a visualization of where
613 migration rates are most likely to depart from the overall mean rate of $\log_{10}(m) = 0$.
614
615 FEEMS is conceptually similar to EEMS but includes a number of modifications that reduce the
616 computational time by several orders of magnitude [14]. Effective migration rates are estimated
617 for each edge (i.e. the connections between vertices), and model parameters are fit using a quasi-
618 Newton optimization algorithm. A smoothing parameter (lambda) is used to encourage nearby
619 edges to have more similar rates. The main output from FEEMS is a map of the point estimates
620 of effective migration rates, relative to the overall mean rate across the area of interest, similar to
621 the map of posterior means from EEMS. However, FEEMS does not produce an equivalent of the
622 exceedance probability map from EEMS.
623
624 To compare the outputs of FEEMS and EEMS, we ran FEEMS with the same 1000-deme grids
625 as above. To assess the effect of grid resolution on model outcomes, with more vertices (demes)
626 than possible in EEMS, we also ran FEEMS using a range of grid resolutions, with edge lengths
627 of 55, 110 and 220 km for each species. To select the smoothing parameter, lambda, we
628 calculated the mean square error from jackknife cross-validation within each set of FEEMS runs.
629 Finally, we visually assessed the resulting maps from each iteration of jackknife cross-validation
630 to assess the robustness of FEEMS estimates to changes at a single deme.

Acknowledgements

This study used WGS data produced by the Ag1000G Project (https://www.malariagen.net/project/ag1000g/) with mosquito specimens contributed by 26 partner studies (https://malariagen.github.io/vector-data/studies-ag1000g.html).

Funding

RSM was supported by NIH award no. K01TW011770. STH and TDO were supported by NIH award no. R01AI145852.

Data Availability

All data analyzed during this study are publicly accessible. Raw sequence reads and sequence read alignments are available on the European Nucleotide Archive under accession number PRJEB42254 (Ag1000G phase 3) and PRJEB2141 (n = 165 *A. gambiae* from DRC); and the NCBI Sequence Read Archive (SRA) under accession number PRJNA1159338 (n = 5 *A. gambiae* from Malawi). Detailed guidance for accessing sample metadata, raw sequence reads, sequence read alignments, and SNP calls is available at https://malariagen.github.io/vector-data/ag3/ag3.0.html.

References

1. Bhatt S, Weiss DJ, Cameron E, Bisanzio D, Mappin B, Dalrymple U, et al. The effect of malaria control on *Plasmodium falciparum* in Africa between 2000 and 2015. Nature. 2015;526:207-11. doi: 10.1038/nature15535.
2. Pryce J, Richardson M, Lengeler C. Insecticide-treated nets for preventing malaria. Cochrane Database Syst Rev. 2018;11(11):CD000363. Epub 2018/11/07. doi: 10.1002/14651858.CD000363.pub3. PMID: 30398672; PMCID: PMC6418392.
3. Tizifa TA, Kabaghe AN, McCann RS, Berg H, Vugt M, Phiri KS. Prevention Efforts for Malaria. Curr Trop Med Rep. 2018;5(1):1-10. doi: 10.1007/s40475-018-0133-y.
4. World Health Organization. World Malaria Report 2023. World Health Organization, 2023.
5. Mutero CM, Kramer RA, Paul C, Lesser A, Miranda ML, Mboera LE, et al. Factors influencing malaria control policy-making in Kenya, Uganda and Tanzania. Malaria Journal. 2014;13(1):305. doi: 10.1186/1475-2875-13-305. PMID: 25107509; PMCID: PMC4249611.
6. Chanda E, Mzilahowa T, Chipwanya J, Mulenga S, Ali D, Troell P, et al. Preventing malaria transmission by indoor residual spraying in Malawi: grappling with the challenge of uncertain sustainability. Malaria Journal. 2015;14:254. doi: 10.1186/s12936-015-0759-3.
7. Tesfazghi K, Traore A, Ranson H, N'Fale S, Hill J, Worrall E. Challenges and opportunities associated with the introduction of next-generation long-lasting insecticidal nets for malaria control: a case study from Burkina Faso. Implement Sci. 2016;11:103. Epub 2016/07/28. doi: 10.1186/s13012-016-0469-4. PMID: 27450082; PMCID: PMC4957273.
8. World Health Organization. Guidelines for malaria vector control. World Health Organization, 2019.
9. World Health Organization. WHO guidelines for malaria, 16 October 2023. World Health Organization, 2023.
10. Bertozzi-Villa A, Bever CA, Koenker H, Weiss DJ, Vargas-Ruiz C, Nandi AK, et al. Maps and metrics of insecticide-treated net access, use, and nets-per-capita in Africa from 2000-2020. Nat Commun. 2021;12(1):3589. Epub 2021/06/13. doi: 10.1038/s41467-021-23707-7. PMID: 34117240; PMCID: PMC8196080.
11. Rousset F. Genetic differentiation and estimation of gene flow from F-statistics under isolation by distance. Genetics. 1997;145(4):1219-28. Epub 1997/04/01. doi: 10.1093/genetics/145.4.1219. PMID: 9093870; PMCID: PMC1207888.
12. Bradburd GS, Ralph PL. Spatial Population Genetics: It's About Time. Annu Rev Ecol Evol Syst. 2019;50(1):427-49. doi: 10.1146/annurev-ecolsys-110316-022659.
13. Petkova D, Novembre J, Stephens M. Visualizing spatial population structure with estimated effective migration surfaces. Nature Genetics. 2015;48(1):1-10. doi: 10.1038/ng.3464.
14. Marcus J, Ha W, Barber RF, Novembre J. Fast and flexible estimation of effective migration surfaces. eLife. 2021;10. Epub 2021/07/31. doi: 10.7554/eLife.61927. PMID: 34328078; PMCID: PMC8324296.
15. Clarkson CS, Miles A, Harding NJ, O'Reilly AO, Weetman D, Kwiatkowski D, et al. The genetic architecture of target-site resistance to pyrethroid insecticides in the African malaria vectors *Anopheles gambiae* and *Anopheles coluzzii*. Mol Ecol. 2021;30(21):5303-17. Epub 2021/02/17. doi: 10.1111/mec.15845. PMID: 33590926; PMCID: PMC9019111.
16. Killeen GF, Knols BG, Gu W. Taking malaria transmission out of the bottle: implications of mosquito dispersal for vector-control interventions. Lancet Infect Dis. 2003;3(5):297-303. Epub 2003/05/03. doi: 10.1016/s1473-3099(03)00611-x. PMID: 12726980.
17. Baber I, Keita M, Sogoba N, Konate M, Diallo MaB, Doumbia S, et al. Population Size and Migration of Anopheles gambiae in the Bancoumana Region of Mali and Their Significance

697 for Efficient Vector Control. PLoS ONE. 2010;5(4):e10270-7. doi:
698 10.1371/journal.pone.0010270.
699 18. North AR, Godfray HCJ. Modelling the persistence of mosquito vectors of malaria in
700 Burkina Faso. Malaria Journal. 2018;17(1):207-15. doi: 10.1186/s12936-018-2288-3.
701 19. Coetzee M, Hunt RH, Wilkerson RC, della Torre A, Coulibaly MB, Besansky NJ.
702 *Anopheles coluzzii* and *Anopheles amharicus*, new members of the *Anopheles gambiae*
703 complex. Zootaxa. 2013;3619(3):246-74. doi: 10.11646/zootaxa.3619.3.2. PMID:
704 10.11646/zootaxa.3619.3.2.
705 20. Irish SR, Kyalo D, Snow RW, Coetzee M. Updated list of *Anopheles* species (Diptera:
706 Culicidae) by country in the Afrotropical Region and associated islands. Zootaxa.
707 2020;4747(3):401-49. doi: 10.11646/zootaxa.4747.3.1.
708 21. Donnelly MJ, Simard F, Lehmann T. Evolutionary studies of malaria vectors. Trends
709 Parasitol. 2002;18(2):75-80. Epub 2002/02/08. doi: 10.1016/s1471-4922(01)02198-5. PMID:
710 11832298.
711 22. Lehmann T, Blackston CR, Besansky NJ, Escalante AA, Collins FH, Hawley WA. The
712 Rift Valley complex as a barrier to gene flow for *Anopheles gambiae* in Kenya: the mtDNA
713 perspective. J Hered. 2000;91(2):165-8. doi: 10.1093/jhered/91.2.165.
714 23. Pinto J, Egyir-Yawson A, Vicente J, Gomes B, Santolamazza F, Moreno M, et al.
715 Geographic population structure of the African malaria vector *Anopheles gambiae* suggests a
716 role for the forest-savannah biome transition as a barrier to gene flow. Evol Appl. 2013;6(6):910-
717 24.
718 24. Simard F, Fontenille D, Lehmann T, Girod R, Brutus L, Gopaul R, et al. High amounts of
719 genetic differentiation between populations of the malaria vector *Anopheles arabiensis* from
720 West Africa and eastern outer islands. Am J Trop Med Hyg. 1999;60(6):1000-9. Epub
721 1999/07/14. doi: 10.4269/ajtmh.1999.60.1000. PMID: 10403334.
722 25. Miles A, Harding NJ, Bottà G, Clarkson CS, Antao T, Kozak K, et al. Genetic diversity of
723 the African malaria vector *Anopheles gambiae*. Nature. 2017;11:11.0.1-9. doi:
724 10.1038/nature24995.
725 26. The *Anopheles gambiae* 1000 Genomes Consortium. Genome variation and population
726 structure among 1142 mosquitoes of the African malaria vector species *Anopheles gambiae*
727 and *Anopheles coluzzii*. Genome Res. 2020;30(10):1533-46. Epub 2020/09/30. doi:
728 10.1101/gr.262790.120. PMID: 32989001; PMCID: PMC7605271.
729 27. Manichaikul A, Mychaleckyj JC, Rich SS, Daly K, Sale M, Chen WM. Robust relationship
730 inference in genome-wide association studies. Bioinformatics. 2010;26(22):2867-73. Epub
731 2010/10/12. doi: 10.1093/bioinformatics/btq559. PMID: 20926424; PMCID: PMC3025716.
732 28. Patterson N, Price AL, Reich D. Population structure and eigenanalysis. PLoS Genet.
733 2006;2(12):e190. Epub 2006/12/30. doi: 10.1371/journal.pgen.0020190. PMID: 17194218;
734 PMCID: PMC1713260.
735 29. Alexander DH, Novembre J, Lange K. Fast model-based estimation of ancestry in
736 unrelated individuals. Genome Res. 2009;19(9):1655-64. doi: 10.1101/gr.094052.109.
737 30. Huestis DL, Dao A, Diallo M, Sanogo ZL, Samake D, Yaro AS, et al. Windborne long-
738 distance migration of malaria mosquitoes in the Sahel. Nature. 2019;574(7778):1-15.
739 31. Li Y, Shetty AC, Lon C, Spring M, Saunders DL, Fukuda MM, et al. Detecting geospatial
740 patterns of *Plasmodium falciparum* parasite migration in Cambodia using optimized estimated
741 effective migration surfaces. International Journal of Health Geographics. 2020;19(1):1-11. doi:
742 10.1186/s12942-020-00207-3.
743 32. Caputo B, Nwakanma D, Caputo FP, Jawara M, Oriero EC, Hamid-Adiamoh M, et al.
744 Prominent intraspecific genetic divergence within *Anopheles gambiae* sibling species triggered
745 by habitat discontinuities across a riverine landscape. Molecular Ecology. 2014;23(18):4574-89.

33. Donnelly MJ, Townson H. Evidence for extensive genetic differentiation among populations of the malaria vector *Anopheles arabiensis* in Eastern Africa. Insect Mol Biol. 2000;9(4):357-67. doi: 10.1046/j.1365-2583.2000.00197.x.
34. Maliti D, Ranson H, Magesa S, Kisinza W, Mcha J, Haji K, et al. Islands and stepping-stones: comparative population structure of *Anopheles gambiae sensu stricto* and *Anopheles arabiensis* in Tanzania and implications for the spread of insecticide resistance. PLoS One. 2014;9(10):e110910. Epub 2014/10/30. doi: 10.1371/journal.pone.0110910. PMID: 25353688; PMCID: PMC4212992.
35. Kamau L, Mukabana WR, Hawley WA, Lehmann T, Irungu LW, Orago AA, et al. Analysis of genetic variability in *Anopheles arabiensis* and *Anopheles gambiae* using microsatellite loci. Insect Mol Biol. 1999;8(2):287-97. Epub 1999/06/24. doi: 10.1046/j.1365-2583.1999.820287.x. PMID: 10380112.
36. Kimura M, Ohta T. The age of a neutral mutant persisting in a finite population. Genetics. 1973;75(1):199-212. Epub 1973/09/01. doi: 10.1093/genetics/75.1.199. PMID: 4762875; PMCID: PMC1212997.
37. Al-Asadi H, Petkova D, Stephens M, Novembre J. Estimating recent migration and population-size surfaces. Plos Genetics. 2019;15(1):e1007908-21. doi: 10.1371/journal.pgen.1007908.
38. O'Connor TD, Fu W, Project NGES, Genetics ESPP, Statistical Analysis Working Group ET, Mychaleckyj JC, et al. Rare variation facilitates inferences of fine-scale population structure in humans. Mol Biol Evol. 2015;32(3):653-60. Epub 2014/11/22. doi: 10.1093/molbev/msu326. PMID: 25415970; PMCID: PMC4327153.
39. Harris DN, Song W, Shetty AC, Levano KS, Cáceres O, Padilla C, et al. Evolutionary genomic dynamics of Peruvians before, during, and after the Inca Empire. Proceedings of the National Academy of Sciences. 2018;115(28):E6526-E35. doi: 10.1073/pnas.1720798115.
40. Shetty AC, Jacob CG, Huang F, Li Y, Agrawal S, Saunders DL, et al. Genomic structure and diversity of *Plasmodium falciparum* in Southeast Asia reveal recent parasite migration patterns. Nature Communications. 2019;10(1):1-11. doi: 10.1038/s41467-019-10121-3.
41. Harris DN, Kessler MD, Shetty AC, Weeks DE, Minster RL, Browning S, et al. Evolutionary history of modern Samoans. Proc Natl Acad Sci U S A. 2020;117(17):9458-65. Epub 2020/04/16. doi: 10.1073/pnas.1913157117. PMID: 32291332; PMCID: PMC7196816.
42. Nait Saada J, Kalantzis G, Shyr D, Cooper F, Robinson M, Gusev A, et al. Identity-by-descent detection across 487,409 British samples reveals fine scale population structure and ultra-rare variant associations. Nat Commun. 2020;11(1):6130. Epub 2020/12/02. doi: 10.1038/s41467-020-19588-x. PMID: 33257650; PMCID: PMC7704644.
43. Sikaala CH, Dlamini B, Lungu A, Fakudze P, Chisenga M, Siame CL, et al. Malaria elimination and the need for intensive inter-country cooperation. a critical evaluation of regional technical co-operation in Southern Africa. Malar J. 2024;23(1):62. Epub 2024/02/29. doi: 10.1186/s12936-024-04891-5. PMID: 38419105; PMCID: PMC10903059.
44. Dennis TPW, Pescod P, Barasa S, Cerdeira L, Lucas ER, Clarkson CS, et al. Cryptic population structure and insecticide resistance in *Anopheles gambiae* from the southern Democratic Republic of Congo. bioRxiv. 2024. doi: 10.1101/2024.03.12.584605.

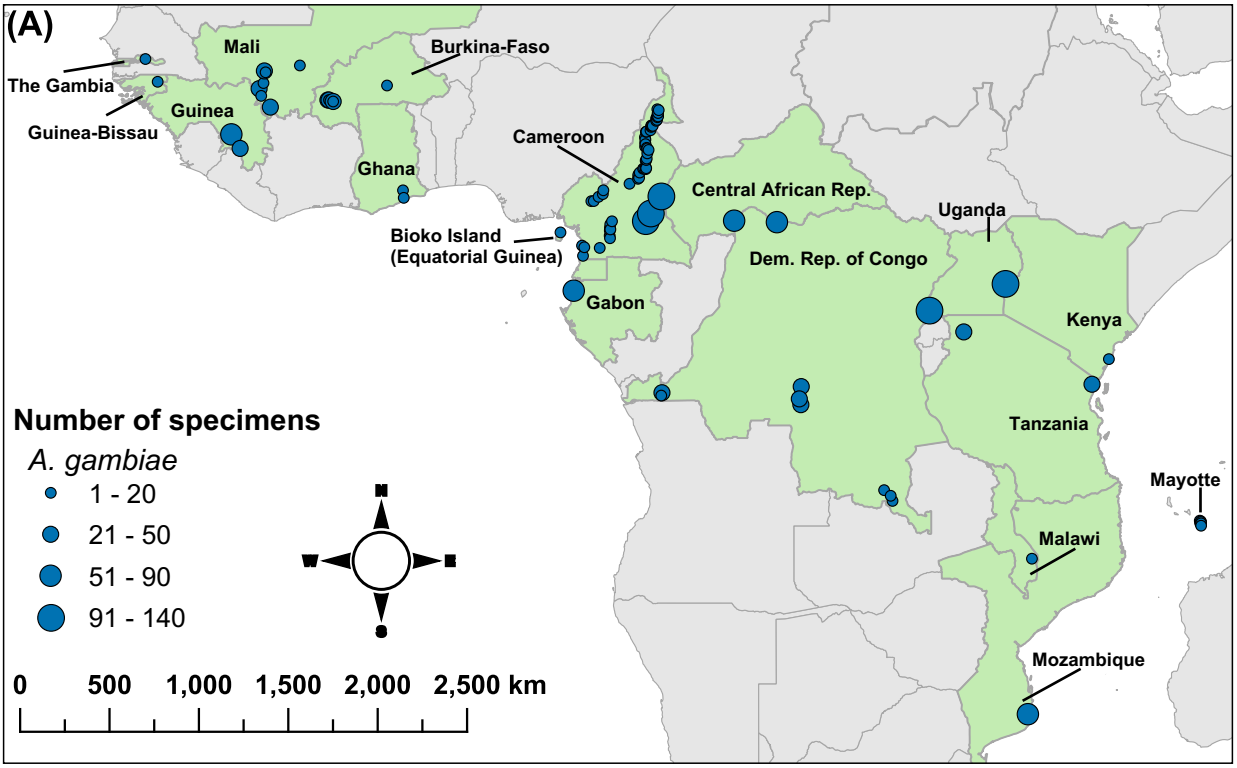
(A)
Mali
Burkina-Faso
The Gambia
Guinea
Guinea-Bissau
Cameroon
Ghana
Central African Rep.
Uganda
Bioko Island
(Equatorial Guinea)
Dem. Rep. of Congo
Gabon
Kenya
Tanzania
Mayotte
Malawi
Mozambique
Number of specimens
A. gambiae
1 - 20
21 - 50
51 - 90
91 - 140
0 500 1,000 1,500 2,000 2,500 km

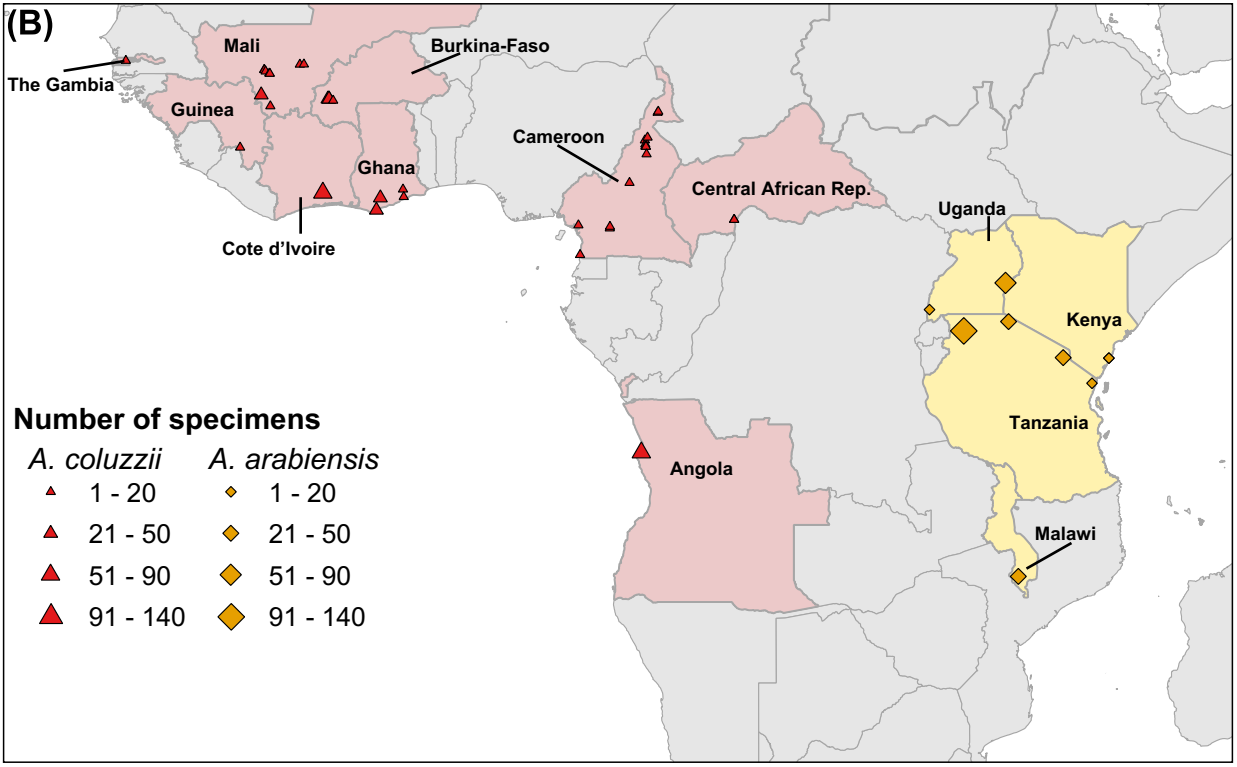
(B)
Mali
Burkina-Faso
The Gambia
Guinea
Cameroon
Ghana
Central African Rep.
Uganda
Cote d'Ivoire
Kenya
Tanzania
Angola
Malawi
Number of specimens
A. coluzzii
1 - 20
21 - 50
51 - 90
91 - 140
A. arabiensis
1 - 20
21 - 50
51 - 90
91 - 140

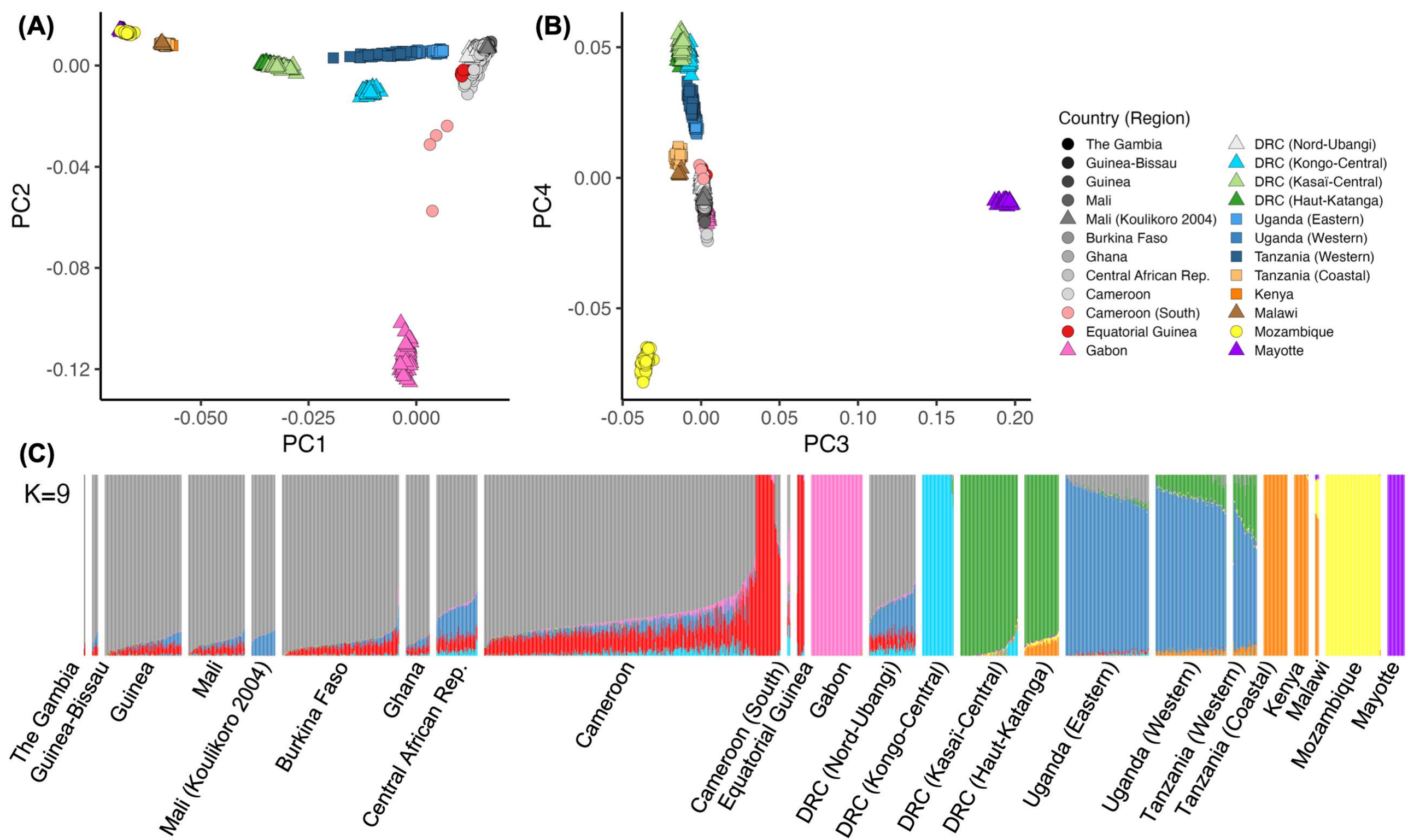
(A)
PC2
PC1
0.00
-0.04
-0.08
-0.12
-0.050
-0.025
0.000
(B)
PC4
PC3
0.05
0.00
-0.05
-0.05
0.00
0.05
0.10
0.15
0.20
Country (Region)
The Gambia
Guinea-Bissau
Guinea
Mali
Mali (Koulikoro 2004)
Burkina Faso
Ghana
Central African Rep.
Cameroon
Cameroon (South)
Equatorial Guinea
Gabon
DRC (Nord-Ubangi)
DRC (Kongo-Central)
DRC (Kasaï-Central)
DRC (Haut-Katanga)
Uganda (Eastern)
Uganda (Western)
Tanzania (Western)
Tanzania (Coastal)
Kenya
Malawi
Mozambique
Mayotte
(C)
K=9
The Gambia
Guinea-Bissau
Guinea
Mali
Mali (Koulikoro 2004)
Burkina Faso
Ghana
Central African Rep.
Cameroon
Cameroon (South)
Equatorial Guinea
Gabon
DRC (Nord-Ubangi)
DRC (Kongo-Central)
DRC (Kasai-Central)
DRC (Haut-Katanga)
Uganda (Eastern)
Uganda (Western)
Tanzania (Western)
Tanzania (Coastal)
Kenya
Malawi
Mozambique
Mayotte

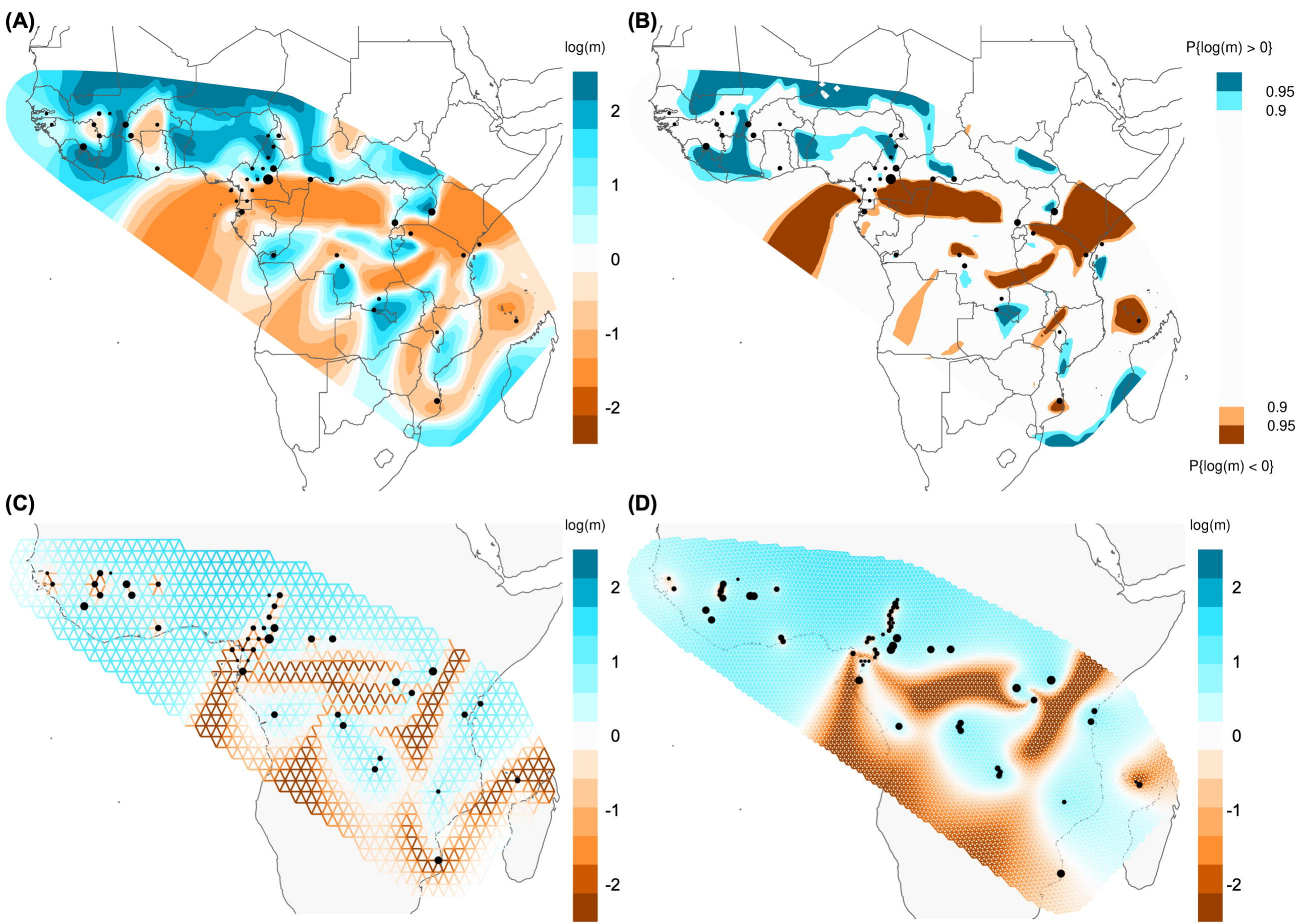
(A)
log(m)
2
1
0
-1
-2
(B)
P{log(m) > 0}
0.95
0.9
0.9
0.95
P{log(m) < 0}
(C)
log(m)
2
1
0
-1
-2
(D)
log(m)
2
1
0
-1
-2

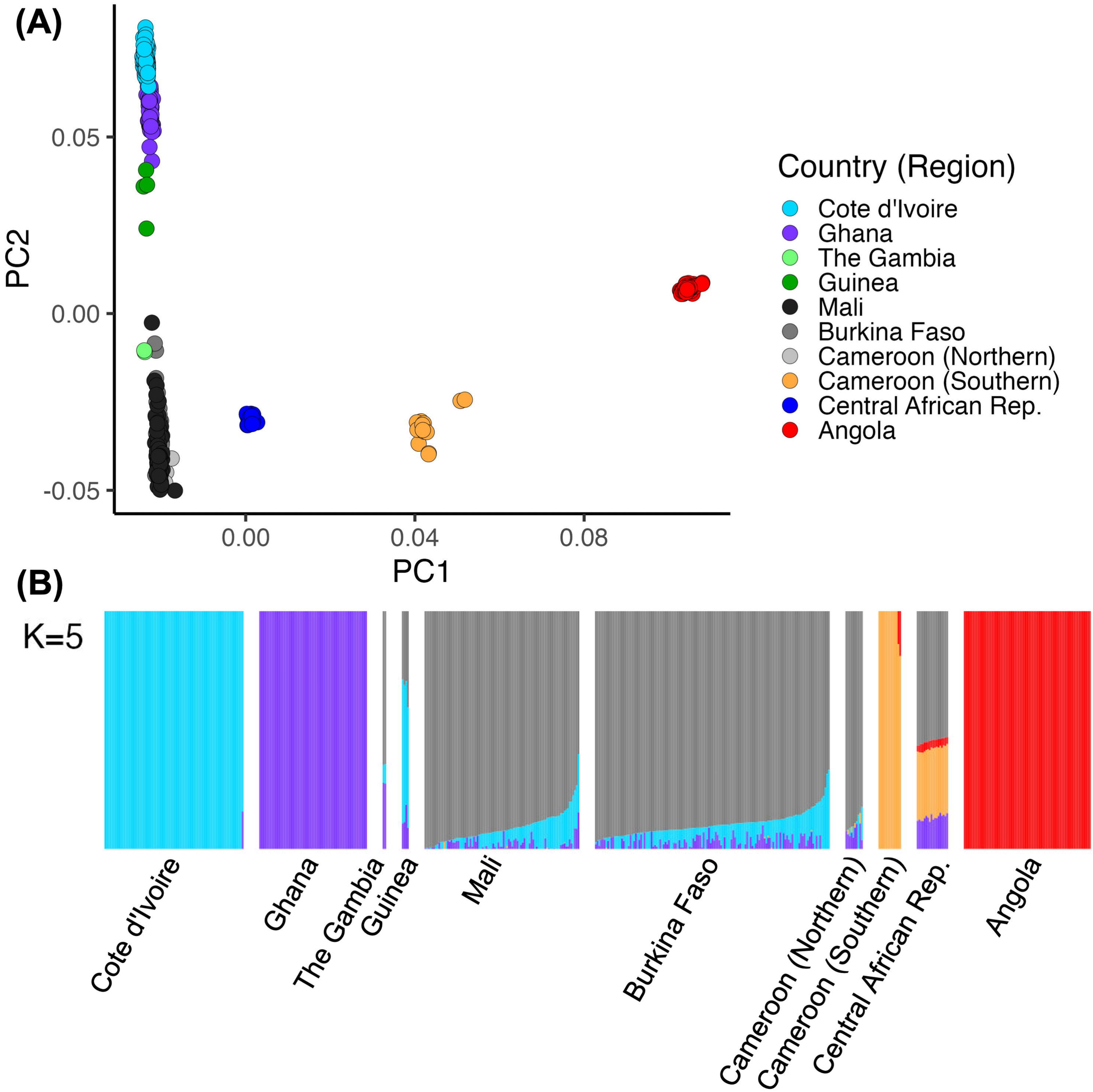
(A)
PC2
0.05
0.00
-0.05
0.00
0.04
0.08
PC1
Country (Region)
Cote d'Ivoire
Ghana
The Gambia
Guinea
Mali
Burkina Faso
Cameroon (Northern)
Cameroon (Southern)
Central African Rep.
Angola
(B)
K=5
Cote d'Ivoire
Ghana
The Gambia
Guinea
Mali
Burkina Faso
Cameroon (Northern)
Cameroon (Southern)
Central African Rep.
Angola

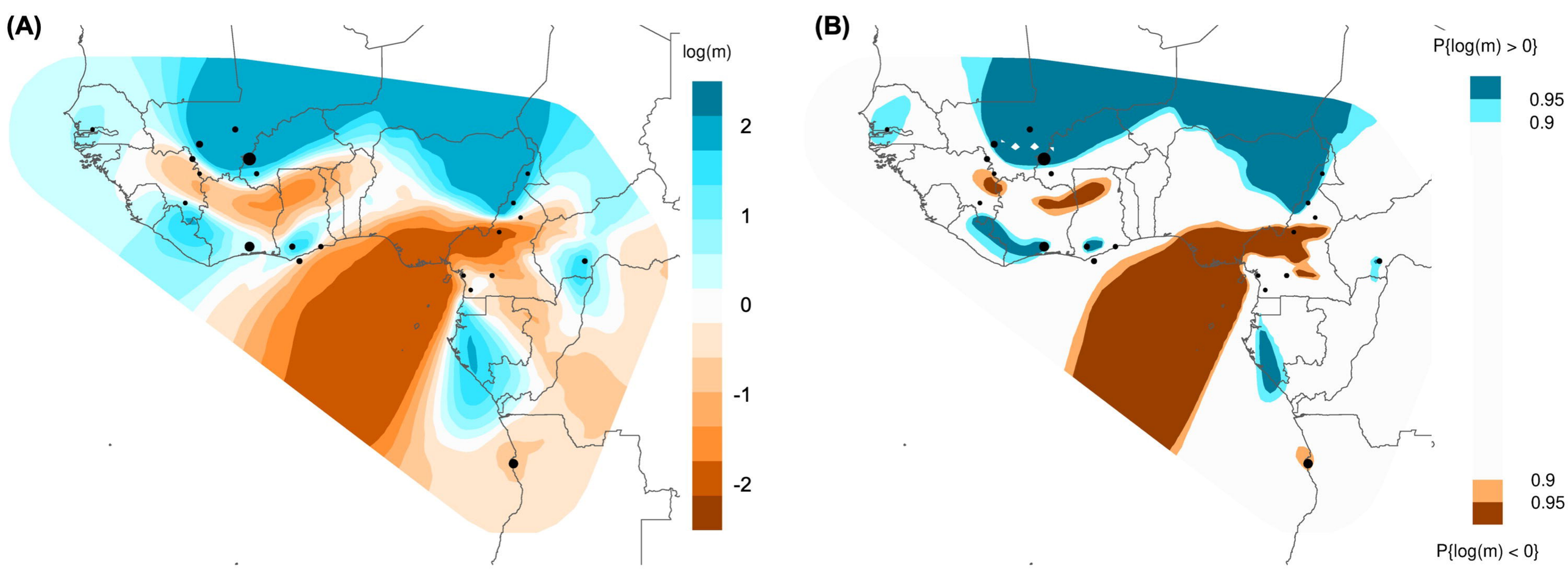
(A)
log(m)
2
1
0
-1
-2
(B)
P{log(m) > 0}
0.95
0.9
0.9
0.95
P{log(m) < 0}

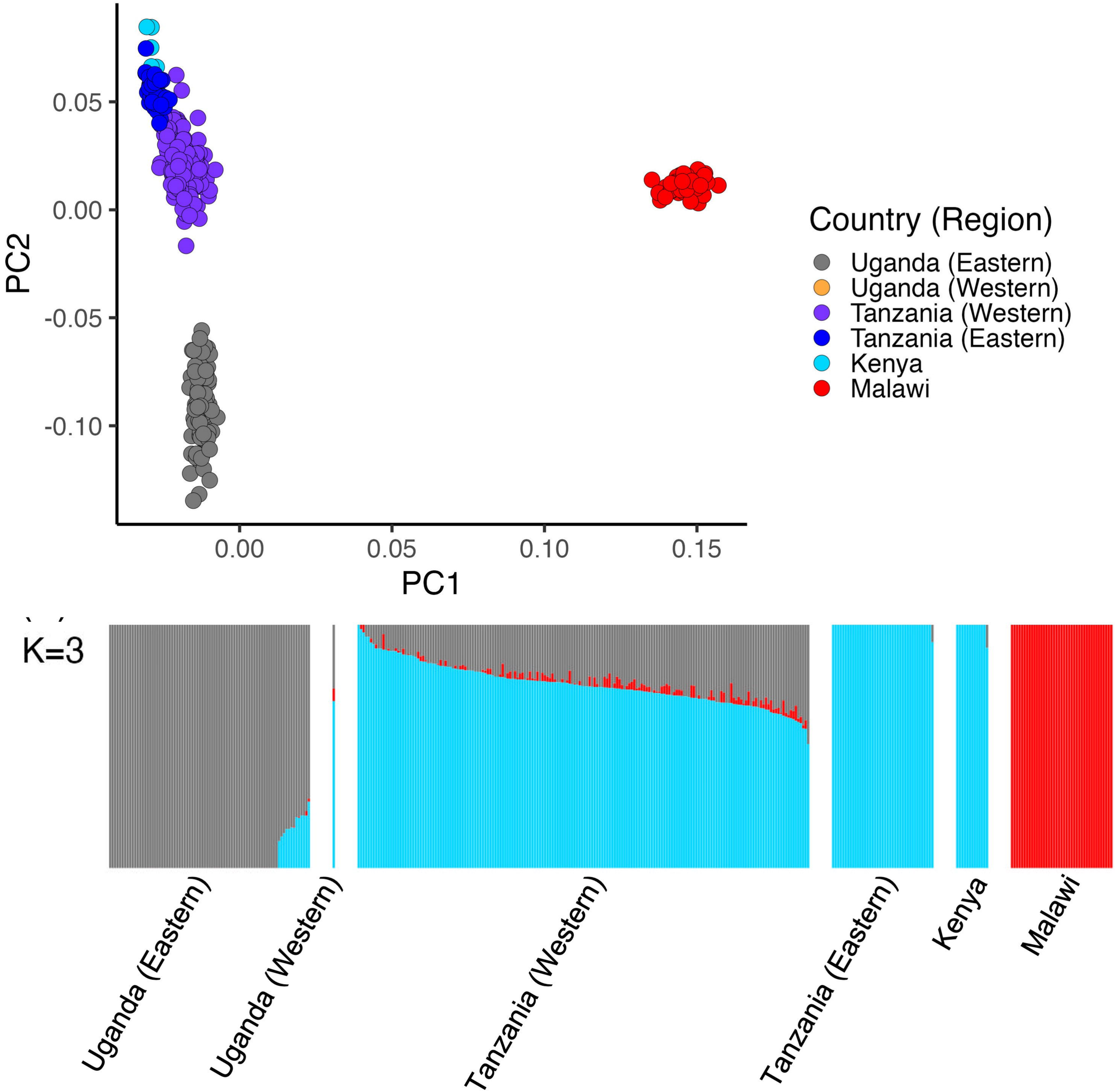
PC2
0.05
0.00
-0.05
-0.10
0.00
0.05
0.10
0.15
PC1
Country (Region)
Uganda (Eastern)
Uganda (Western)
Tanzania (Western)
Tanzania (Eastern)
Kenya
Malawi
K=3
Uganda (Eastern)
Uganda (Western)
Tanzania (Western)
Tanzania (Eastern)
Kenya
Malawi

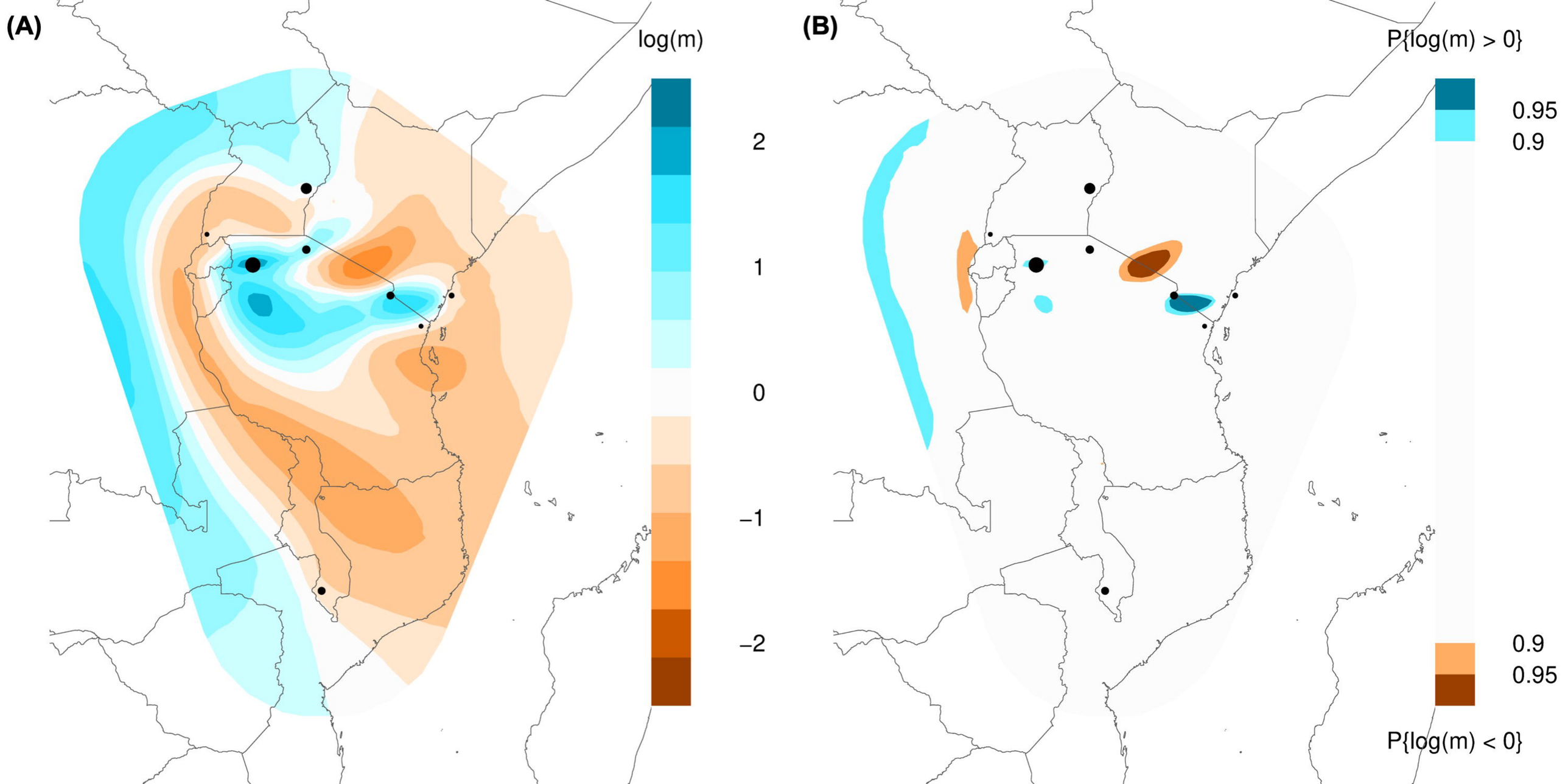
(A)
log(m)
2
1
0
−1
−2
(B)
P{log(m) > 0}
0.95
0.9
0.9
0.95
P{log(m) < 0}